Numerical modelling of aerosol dispersion inside a rotating aerosol chamber

by

Magnus Vartdal

THESIS

for the degree of

MASTER OF SCIENCE

(Master i Anvendt matematikk og mekanikk)

Faculty of Mathematics and Natural Sciences
University of Oslo

May 2009

Det matematisk- naturvitenskapelige fakultet
Universitetet i Oslo

Abstract

Numerical simulations of the airflow inside a slowly rotating aerosol chamber is carried out using a high resolution LES and several RANS based turbulence models. The results of the LES revealed a complex turbulent flow field which none of the RANS models were able to faithfully reproduce. The predicted secondary flow where however similar in magnitude as well as holistic character. Simulations of passive aerosol tranport based on the RANS flow fields did reveal that they possibly can be used for this purpose, as the results did not contradict observations of the aerosol deposition.

Acknowledgement

First and foremost, many thanks to my supervisor Bjørn Anders Petterson Reif at the University of Oslo and the Norwegian Defence Research Establishment(FFI). His guidance has been very helpful throughout the project.

I further wish to thank Emma M. M. Wingstedt and the other researchers at FFI for helpuful comments and useful discussions.

My fellow student Hannibal Fossum has provided me with many an enlightening discussion, good ideas and welcome companionship.

Finally, I wish to thank my family for being so supportive and patient.

Contents

Chapter 1

Introduction

1.1 Background

The problem of dispersion is an intriguing problem because of its fundamental scientific nature as well as its practical interest in fields such as enviromental science and engineering. Many compounds are dispersed in the form of aerosols, which are small particles or droplets suspended in a gas, the exact nature of the dispersion obviously depend on the physical properties of the aerosol. In many cases, especially when microorganisms are involved, the properties of the aerosols are functions of time. In order to effectively predict the dispersion it is thus vital to study the long time behaviour of the aerosols under controlled circumstances. To accomplish this specially designed aerosol chambers are employed. In order to be effective these chambers need to be able to maintain a sufficient amount of aerosols suspended in the gas for a sufficient amount of time. This is a significant challenge and one common approach has been to apply stirring, (usually in the form of fans) to ambient air in an attempt to balance the gravitational settling of the aerosols [1]. Another, and perhaps more sucessful, approach has been to construct a low aspect ratio cylindrical chamber that is slowly rotating about an horizontal axis. In fact, rotating aerosol chambers have been found to be an effective apparatus for this purpose, with very low gravitational settling [2] [3]. The rotating walls inside the enclosed cylinder creates a three dimensional flow pattern that carries the aerosols in a spiraling motion within the chamber, keeping them airborne for tens of hours. The slowly rotating environment within the chamber also counteracts the gravitational settling effect, keeping it to minimum.

The dominant feature to accurately determining the transport of aerosols inside the chamber is obviously the flow field itself. Previous models used to study this confirguration [4] [5] have been based on the assumption that the fluid flow inside the chamber is entirely laminar. It is unlikely that this assumption constitutes a physically sound approximation due to the formation of turbulent boundary layers along the walls for all but the slowest rates of rotation.

An important objective of the present study has been to investigate in detail the flow field in such chambers.

The motivation for this study is to characterize the transport of aerosols within the chamber and estimating the rate of deposition of aerosols on the chamber walls.

1.2 The aerosol chamber

In this paper an existing rotating aerosol chamber, 2 feet wide and 6 feet in diameter, is considered [2]. The chamber was created to study the airborne viability of bacteria. It contains air at atmospheric pressure and rotates steadily at 5 rounds per minutes(rpm) about the cyllindrical axis, which is horizontally alligned. Inside the chamber are devices for injecting the aerosols, collecting samples as well as a wedge. These features have, for simplicity, been neglected in the model used in this paper. Thus the chamber can be represented geometrically by a cylinder which is depicted in figure 1.1

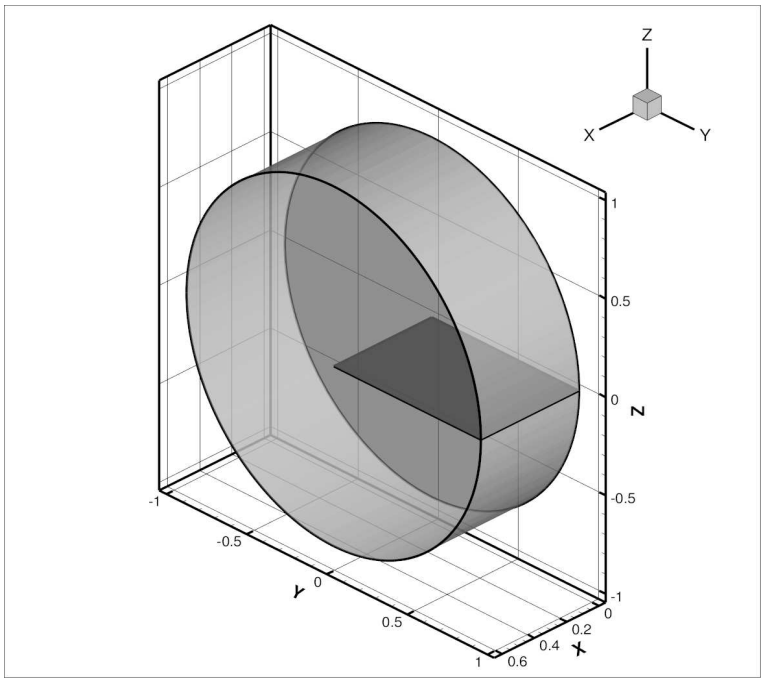

Figure 1.1: Geometric representation of the Aerosol Chamber. The x-axis is the rotational axis. The surface contained by the shaded square is not a feature of the domain. It only indicates the computational domain used in the RANS case.

1.3 Objectives

This thesis is primarily concern with numerical simulation of the flow field inside a steadily rotating axisymmetric chamber. Turbulent conditions are expected but the imposed rotation will affect the turbulence in a complex way. Additionally the relatively low Reynolds number makes this a challenging case to model, as turbulence models in general have difficulty with predicting these kinds of flows. Because of this several different models have been considered.

The actual transport of the aerosols is also investigated, but as this is entirely dependent on a good estimation of the flow field it was considered a secondary goal. The objectives of the thesis can be summarized as follows:

- Employ models based on the Reynolds Averaged Navier-Stokes appraoch to simulate the flow field inside the chamber
- Employ the Large Eddy Simulation approach to simulate the flow field inside the chamber and provide a set of reference data for verification of the simpler RANS approach.
- Investigate the use of Lagrangian and Eulerian based aerosol transport models.

This thesis is divided into several Chapters. In Chapter 2 the theory behind the different modelling approaches is discussed. In Chapter 3 the numerical aspects of the study is described. In Chapter 4 the results of the simulations are considered and in Chapter 5 the concluding remarks are given.

Chapter 2

Theory

2.1 Notation

In this remainder of this text, we adopt index notation for vectors and tensors. This means that if an index(marked by a subscript e.g. $_i$) appears once in each term, the equation is valid for all values of the index (in this text that will be 1, 2 and 3). Such an index is called a *free index*. One free index indicates a first order tensor(vector), two free indicies denotes a second order tensor and so on. If an index appears twice in a term, it is summed over for all possible values of the index. For example: $x_i x_i = x_1^2 + x_2^2 + x_3^2$. Such an index is called a *dummy index*. In addition, I will use the abbreviation $\partial_i = \frac{\partial}{\partial x_i}$, where x_i denotes a spatial variable. Furthermore, if slightly inconsistently, we will use the abbreviation $\partial_t = \frac{\partial}{\partial t}$ to denote the temporal derivative.

2.2 Turbulent Flow

In the introduction it was stated that the flow inside the chamber is turbulent, so before we continue into the theory on how it is modelled a few words on the nature of turbulence is in order.

Turbulence is a state of fluid flow that is dominated by seemingly random velocity fluctuations. Its very nature appears chaotic, but in spite of that several characteristics that are common to all turbulent flows can be found, and among them are [6] :

- High Reynolds number $Re = \frac{UL}{\nu} \gtrsim 10^3$ where U is a characteristic velocity scale, L is a characteristic length scale and ν is the kinematic viscosity of the fluid.

- Diffusive, it has a rapid transport/mixing property. Meaning that it rapidly transports quantities such as momentum, temperature, kinetic energy etc.

- Dissipative, meaning that the turbulent energy is transformed into inertial energy by the viscous stresses.
- Three dimensional. Turbulence cannot sustain itself in one or two dimensions.
- Vortical flow structures. Turbulence contains 'whorls' of various length scales.
- Satisfies the continuum hypothesis, meaning that the shortest scales are much larger than the mean free path.

It is important to remember that these characteristics are properties of the flow, and not of the fluid. Thus, turbulence must be viewed as a flow regime, not as a material property. If the flow is not turbulent it is called laminar.

Wheteher the flow is laminar or turbulent it is governed by the Navier-Stokes equations and the mass conservation equation(collectively often refered to as the Navier-Stokes equations), along with certain constitutive relations. A derivation of the Navier-Stokes equations can be found in any introductory book on fluid mechanics such as[7].

2.3 The governing equations

The fluid flow inside the aerosol chamber is governed by the Navier-Stokes equations for an incompressible Newtonian fluid and the mass conservation equation. In a constantly rotating frame of reference, when gravity is neglected, these can be expressed as:

$$\partial_t \tilde{u}_i + \tilde{u}_j \partial_j \tilde{u}_i = -\frac{1}{\rho}\partial_i \tilde{p} + \nu \partial_j \partial_j \tilde{u} - (\Omega_j x_j \Omega_i - \Omega_j \Omega_j x_i) - 2\Omega_l \tilde{u}_k \epsilon_{lki} \tag{2.1}$$

$$\partial_i \tilde{u}_i = 0 \tag{2.2}$$

Here, $\tilde{u}$ and $\tilde{p}$ are the velocity and pressure fields, ρ is the density of the air, ν is the kinematic viscosity of air,x is the position vector, Ω_j is the angular velocity of the reference frame about the x_j axis and ϵ_{lki} is the cyclic permutation tensor which is defined by:

$$\epsilon_{lki} = \begin{cases} 1, & if \quad lki = 123, 231, 312 \\ -1, & if \quad lki = 321, 132, 213 \\ 0, & otherwise \end{cases}$$

When we compare these equations to that of one in a inertial reference frame, the differnce consists of two effects. These are the centrifugal force, $-(\Omega_j x_j \Omega_i - \Omega_j \Omega_j x_i)$, which is the result of the inertia effect described by Newton's first law

and the coriolis force, $-2\Omega_l \tilde{u}_k \epsilon_{lki}$, which is a similar effect that only applies to objects in relative motion to the rotating reference frame.

There exists no general analytic solution to the Navier-Stokes equations. Given a precise set of boundary and initial conditions it is however possible to solve the equations numerically with what we call a direct numerical simulation(DNS). This is however extremely computationally demanding, and furthermore it is practically impossible to obtain exact initial and boundary conditions. Thus, to get any further, we need some sort of turbulence model.

2.4 Reynolds Averaged Navier-Stokes Equations

In the Reynolds Averaged Navier-Stokes approach the exact description of the flow field featured in the Navier-Stokes equations is substituded by a statistical description. Instead of solving equations for the exact flow fields we solve equations for the mean flow fields. To develop these equations we need the concept of an ensemble average.

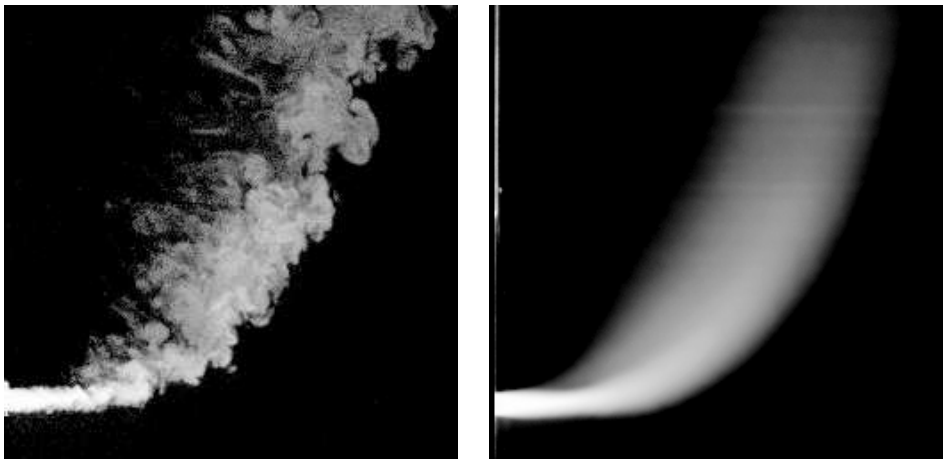

(a) Instantaneous (b) Averaged

Figure 2.1: Instantaneous and time averaged views of a jet in cross flow. The jet exits from the wall at the left in to a stream flowing from bottom to top(Su& Mungal 1999)

An ensemble average is formally defined as:

$$x_{avg} = \frac{1}{N} \sum_{i=1}^{N} x_i$$

where the x_i's are independent realisations of a random variable.

The mean of a random variable is then defined as:

$$\overline{x} = \lim_{N\to\infty} \frac{1}{N} \sum_{i=1}^{N} x_i$$

The ensemble average has the following properties:

- Linearity: $\overline{x+y} = \overline{x} + \overline{y}$
- Average of average: $\overline{\overline{x}} = \overline{x}$

To obtain an actual ensemble average for a flow field, one would carry out the same experiments many times and measure the realisations of the variables each time. By using an ensemble average we ensure that we can model statistically unsteady flow. A statistically unsteady flow is a flow in whitch the statistics are functions of time.

If the statistics are independent of time the flow is called statistically stationary and in this case the ensemble average is equal to a time average.

In order to develop the equations for the mean flow the Reynolds decomposition is introduced. This means that the velocity and pressure fields are split in to a mean and fluctuating part:

$$\tilde{u_i}(\mathbf{x}, t) = U_i(\mathbf{x}, t) + u_i(\mathbf{x}, t)$$

$$\tilde{p}(\mathbf{x}, t) = P(\mathbf{x}, t) + p(\mathbf{x}, t)$$

Where U_i and P denotes the mean fields and u_i and p denotes the fluctuating fields. In terms of the ensemble averaging this means that the following relations hold. $U_i = \overline{\tilde{u_i}}$, $P = \overline{\tilde{p}}$, $\overline{u_i} = 0$ and $\overline{p} = 0$.

If we now insert the Reynolds decomposition into (2.1) and (2.2) and take the ensemble average we arrive at the Reynolds Averaged Navier-Stokes Equations(RANS):

$$\partial_t U_i + U_j \partial_j U_i = -\frac{1}{\rho}\partial_i P + \nu \partial_j \partial_j U_i - (\Omega_j r_j \Omega_i - \Omega_j \Omega_j r_i) - 2\Omega_l U_k \epsilon_{lki} - \partial_j(\overline{u_i u_j}) \quad (2.3)$$

$$\partial_i U_i = 0 \quad (2.4)$$

In (2.3) we see that the only term where fluctuating quantities are present is the last term. This term is called the *Reynolds stress tensor*. It originates in the original advection term $\tilde{u_j}\partial_j\tilde{u_i}$. We arrive at this form from $\overline{u_j \partial_j u_i}$ by noting that (2.2)-(2.4) yields $\partial_i u_i = 0$ and the chain rule thus implies the form found in (2.3).The Reynolds stresses are not really stresses, but they are so termed because they have the same dimensions as the viscous stress. Physically, they represent the averaged effect of turbulent advection on the mean flow field.

The Reynolds stress tensor is a problem because of the fact that the average of two fluctuating quantities in general is non zero. Thus we are faced with an

additional 6 unknowns(due to symmetry $\overline{u_i u_j} = \overline{u_j u_i}$), bringing the total number of unknowns in the RANS equations to 10. This is a problem since we only have 4 equations! Clearly, we need some sort of closure relation, but how this should be formulated is not at all clear.

2.4.1 The Reynolds Stress Transport Equation

Before we adress the issue of closure, we first derive a transport equation for the Reynolds Stresses. To do this we first subtract the RANS equations (2.3) from the Navier-Stokes equations (2.1) to obtain an equation for the fluctuating part of the velocity field:

$$\partial_t u_i + U_k \partial_k u_i + \partial_k (u_k u_i - \overline{u_k u_i}) = -\frac{1}{\rho}\partial_i p + \nu \partial_k \partial_k u_i - 2\Omega_l u_k \epsilon_{lki} \tag{2.5}$$

We now multiply by u_j, take the average and add the transpose equation to obtain the Reynolds Stress Transport Equation(RSTE):

$$\begin{aligned}
\partial_t \overline{u_i u_j} + U_k \partial_k \overline{u_i u_j} = & -\frac{1}{\rho}(\overline{u_j \partial_i p} + \overline{u_i \partial_j p}) && \text{pressure redistribution} \\
& - \partial_k \overline{u_k u_i u_j} && \text{Turbulent transport } d_{ij}^t \\
& - 2\nu \overline{\partial_k u_i \partial_k u_j} && \text{viscous dissipation } \varepsilon_{ij} \\
& - \overline{u_i u_k}\partial_k U_j - \overline{u_j u_k}\partial_k U_i && \text{production } P_{ij} \\
& + \nu \partial_k \partial_k \overline{u_i u_j} && \text{molecular diffusion} \\
& - 2\Omega_l(\overline{u_i u_k}\epsilon_{lkj} + \overline{u_j u_k}\epsilon_{lki}) && \text{rotational production } R_{ij}
\end{aligned} \tag{2.6}$$

The left hand side describes the total rate of change, and the physical interpretations of the terms on the right have been included. These equations are not a closed set of equations for the Reynolds stresses as the pressure redistribution, the turbulent transport and the viscous dissipation contain unknown correlations. This means that simply inserting the RSTE into the RANS equations will not help us close the problem. This is however not a futile exercise, since we by considering what the terms in the RSTE can gain some insight into what mechanisms that are involved in the evolution of the Reynolds stresses.

Note that the effect of system rotation is to introduce an additional production term R_{ij}.

2.4.2 Turbulence kinetic energy

Another useful concept in the formulation of the closure models is that of turbulence kinetic energy. It represents the amount of energy stored in the turbulent

fluctuations and is defined by

$$k = \frac{1}{2}\overline{u_i u_i} \tag{2.7}$$

which is half the trace of the Reynolds Stress Tensor.

We can deduce a transport equation for k from the Reynolds Stress transport equation (2.6) by index contraction. That is, we set j=i and apply the rules of index notation. This results in the turbulence kinetic energy equation(TKE)

$$\begin{aligned}
\partial_t k + U_j \partial_j k = &-\frac{1}{\rho}\partial_i \overline{u_i p} && \text{pressure diffusion } d^p \\
&-\frac{1}{2}\partial_j \overline{u_j u_i u_i} && \text{Turbulent transport } d^t \\
&-\nu\overline{\partial_j u_i \partial_j u_i} && \text{viscous dissipation } \varepsilon \\
&-\overline{u_i u_j}\partial_j U_i && \text{production } P \\
&+\nu\partial_j\partial_j k && \text{molecular diffusion}
\end{aligned} \tag{2.8}$$

We see that the rotational 'production' term does not appear in this equation as it only redistributes energy among the Reynolds stresses($R_{ii} = 0$). This means that the effect of rotational production is excluded in any model based on scalar variables! With these concepts we are now ready to adress the issue of how to close the RANS equations.

2.5 Closure Models

As stated earlier, general RANS equations have a total of 10 unknowns. The unknowns are:

- The 3 mean velocity components
- The mean pressure
- The 6 indepenent components of the Reynolds stress tensor $\overline{u_i u_j}$.

Since we have 4 equations at our disposal we see that some sort of closure model is required, and since the RANS equations are an attempt to solve for the mean fields, it is natural to try to model the Reynolds stresses in terms of known quantities. But which quantities can we use? As stated earlier, turbulence is a property of the flow, not of the fluid, thus it is apparent that we should only use quantities related to the flow (such as velocity) and not quantities related to the material (such as viscosity). Another requirement is that of galilean invariance, meaning that the model should be the same in all inertial frames of reference. This puts further restrictions on our choice of quantities to be used in modeling the

Reynolds stresses, since, among other things the velocity is not galilean invariant. One quantity that is galilean invariant is the mean rate of strain tensor, and it is defined by:

$$S_{ij} = \frac{1}{2}(\partial_j U_i + \partial_i U_j)$$

The mean rate of strain tensor is the starting point of the Boussinesq eddy viscosity model, which is a basis for many turbulence models.

2.5.1 The Boussinesq eddy viscosity hypothesis

The Boussinesq eddy viscosity hypothesis was developed by Boussinesq in 1877. It assumes that the Reynolds stress tensor can be expressed as $\overline{u_i u_j} = f(\delta_{ij}, S_{ij})$, where δ_{ij} is the kronecker delta defined by

$$\delta_{ij} = \begin{cases} 1, & if \quad i = j \\ 0, & if \quad i \neq j \end{cases}$$

It further assumes that the function is linear so that we get:

$$\overline{u_i u_j} = \alpha \delta_{ij} + \beta S_{ij}$$

From the definition of the turbulence kinetic energy, it is clear that $\overline{u_i u_i} = 2k$, which implies:

$$\overline{u_i u_i} = 3\alpha = 2k$$
$$\Rightarrow \alpha = \frac{2k}{3}$$

Where we have used the fact that $S_{ii} = 0$, which is easily confirmed by the application of mass conservation.

Now, if we consider the dimensions of the Reynolds stress $\overline{u_i u_j} : [\frac{m^2}{s^2}]$ and the mean rate of strain tensor $S_{ij} : [s^{-1}]$ it is apparent that $\beta : [\frac{m^2}{s}]$, which is a viscosity. It is thus appropriate to defined an eddy viscosity ν_T. In accordance with Boussinesq we then define:

$$\beta = -2\nu_T$$

Which mean that we end up with the following linear eddy viscosity model:

$$\overline{u_i u_j} = \frac{2}{3} k \delta_{ij} - 2\nu_T S_{ij} \tag{2.9}$$

It is important to note that ν_T is still unknown and has to be modelled. However we have made some progress as the number of unknowns has been reduced from six to one!

There exists quite a few turbulence models based on the eddy viscosity hypothesis. One usual way of classifying these models is by the number of additional equations they solve in order to close the equations.

At this point the development of two eddy viscosity based models are included. The model are the 0-equation mixing length model and the 2-equation $k-\varepsilon$ model. The mixing length model is included because it illustrates the rationale behind the closure model used in the LES case. The development of the $k-\varepsilon$ model is included as it is the basis for the $\overline{v^2}-f$ model used in this paper. Furthermore, it serves as an illustration of some of the common methods used in the modelling of many transport equations.

Prandtl's mixing length model

Prandtl proposed his mixing length model in 1925. It is based on the assumption that turbulent fluctuations are caused by displacement of mean momentum. If we consider shear flow, then a fluctuation caused by a small displacement l' in the y-direction is given by:

$$u = U(y + l') - U(y) \approx l'\partial_y U$$

From this it follows that if the fluctuations are mainly in the x-direction then:

$$k = \frac{1}{2}\overline{u_i u_i} \propto \overline{l'^2}|\partial_y U|$$

We now define the mixing length by $l_m^2 = \overline{l'^2}$. The next step is to find an equation for the eddy viscosity, and as we did in the Boussinesq case we use dimensional argument. Since $l_m : [m]$ and$\partial_y U : [s^{-1}]$ it is clear that $\nu_T \propto l_m^2 \partial_y U$. Prandtl thus used:

$$\nu_T = l_m^2 |\partial_y U|$$

If we insert these two approximations into the linear eddy-viscosity hypothesis we have reduced the problem of closing the equations to the simpler problem of determining the mixing length l_m. This can be done, but the value of l_m will depend on the geometry.

$k-\varepsilon$ model

The starting point of the $k-\varepsilon$ model is the RANS-equations with the additional assumption of the linear eddy viscosity hypothesis. Thus, what remain is to model is ν_T. To accomplish this we attempt to use the transport equation for turbulence kinetic energy(2.8) which with the symbols defined earlier becomes:

$$\frac{Dk}{dt} = P - \varepsilon + d^t + d^p + \nu\partial_j\partial_j k$$

In this equation the unknown terms are turbulent transport (d^t), pressure diffusion(d^p) and dissipation(ε), and so we need to model these as well!

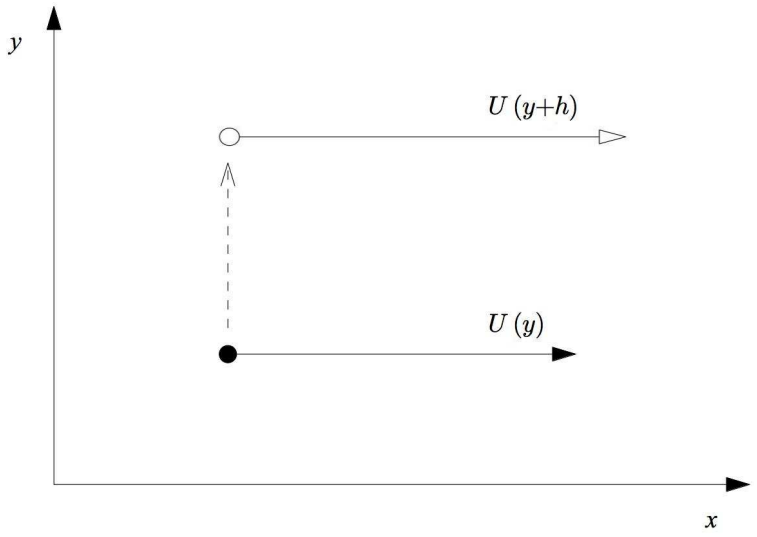

Figure 2.2: The mixing length rationale

The pressure diffusion and turbulent transport terms are both transport terms, and so we model them together by a gradient transport model:

$$d^k = -\partial_j(\frac{\nu_T}{\sigma_k}\partial_j k)$$

where σ_k is a constant and so we have:

$$\frac{Dk}{dt} = P - \varepsilon + \nu\partial_j\partial_j k + \partial_j(\frac{\nu_T}{\sigma_k}\partial_j k) \tag{2.10}$$

This leaves the dissipation which we seek to model by its own transport equation. To this end, let us consider homogeneous turbulence. Homogeneous turbulence is a state in which correlations of fluctuating quantities is constant in space. If this is the case the transport terms disappear from (2.8)(remember that k is also a correlation) and we are left with:

$$\frac{dk}{dt} = P - \varepsilon$$

Now, in homogeneous turbulence there exists a state called structural equilibrium in which the turbulent timescale is constant. From dimensional arguments, it is clear that $\frac{k}{\varepsilon}$ is such a timescale and thus structural equilibrium implies $\frac{d}{dt}(\frac{k}{\varepsilon}) = 0$. The chain rule then gives:

$$\frac{1}{\varepsilon}\frac{dk}{dt} + k\frac{d}{dt}(\frac{1}{\varepsilon})$$
$$\Rightarrow \frac{1}{\varepsilon}\frac{dk}{dt} = \frac{k}{\varepsilon^2}\frac{d\varepsilon}{dt}$$

$$\Rightarrow \frac{d\varepsilon}{dt} = \frac{1}{k/\varepsilon}\frac{dk}{dt}$$

Seeing as this is valid for structural equilibrium we attempt to generalize it towards an equation valid in all cases. To this end we suggest:

$$\frac{D\varepsilon}{dt} = \frac{C_{\varepsilon 1}P - C_{\varepsilon 2}\varepsilon}{k/\varepsilon} + \nu\partial_j\partial_j\varepsilon + d^{\varepsilon} \tag{2.11}$$

Where $C_{\varepsilon 1}$ and $C_{\varepsilon 2}$ are constants and $d^{\varepsilon} = \partial_j(\frac{\nu_T}{\sigma_\varepsilon}\partial_j\varepsilon)$ is a gradient diffusion analogous to d^k.

With this equation for the dissipation we have everything we need to obtains an equation for the eddy-viscosity. For by dimensional arguments it is clear that $\nu_T \propto \frac{k^2}{\varepsilon}$. So we conclude that:

$$\nu_T = C_\mu \frac{k^2}{\varepsilon} \tag{2.12}$$

This means that the RANS equations along with the relations (2.10), (2.11) and (2.12) is a closed set of equations, and the only thing that remains is to determine the model coefficients: $C_{\varepsilon 1}$,$C_{\varepsilon 2}$, C_μ ,σ_k and σ_ε. These constants can be found by conducting a series of experiments which will not be described here.

2.5.2 Differential Reynolds Stress Models

An alternative to the eddy viscosity hypothesis is a differential Reynolds Stress model. In this approach one does not attempt to close the RANS equations directly. Instead an attempt is made to model the unclosed terms in the RSTE 2.6. This is a more complex alternative, which has several advantages. Among the greatest advantages is that we are now using tensor variables to represent the turbulence. This means that we are better able to account for the anisotropy of the Reynolds Stresses. A spesific advantage for this case is that we now are able to include the effect of rotational production into our model.

From section 2.4.1 we know that there are three terms that need to be modelled in order to close the RSTE. Those are the turbulent transport d^t_{ij}, the viscous dissipation ε_{ij} and the pressure redistribution. For modelling purposes the pressure redistribution is often divided into a redistributive part and a transport part by applying the chain rule:

$$-\frac{1}{\rho}(\overline{u_j\partial_i p} + \overline{u_i\partial_j p}) = -\frac{1}{\rho}(\overline{\partial_j(u_i p)} + \overline{\partial_i(u_j p)}) + \frac{1}{\rho}\overline{p(\partial_j u_i + \partial_i u_j)} \tag{2.13}$$

where

$$d^p_{ij} = -\frac{1}{\rho}(\overline{\partial_j(u_i p)} + \overline{\partial_i(u_j p)})$$

is the pressure transport term, and

$$\Phi_{ij} = \frac{1}{\rho}\overline{p(\partial_j u_i + \partial_i u_j)}$$

is the redistribution term known as the pressure strain. As it is a redistribution term, the effect of Φ_{ij} is another effect that scalar model can't account for.

2.5.3 The closure models

In this project several closure models where used, but suitably convergent solutions were achived only for three models. The models were the 1-equation Spalart-Allmars model the 4-equation $\overline{v^2}-f$ model and the Low-Re Stress Omega differential stress model. The details of each closure model is presented in the following.

The Spalart-Allmaras model

The Spalart-Allmaras model [8] is an eddy viscosity type model which solves an additional transport equation for a modified form of the turbulent kinematic viscosity. This transport equation takes the following form:

$$\partial_t\tilde{\nu} + U_i\partial_i\tilde{\nu} = G_{\tilde{\nu}} + \frac{1}{\sigma_{\tilde{\nu}}}\left[\partial_i\left((\nu+\tilde{\nu})\partial_i\tilde{\nu} + C_{b2}(\partial_i\tilde{\nu})^2\right] - Y_{\tilde{\nu}} \tag{2.14}$$

where $\sigma_{\tilde{\nu}}$ and C_{b2} are constants. $G_{\tilde{\nu}}$ and $Y_{\tilde{\nu}}$ are the production and destruction of modified turbulent kinematic viscosity.

The turbulent kinematic viscosity is computed from $\tilde{\nu}$ according to the following relation:

$$\nu_T = \tilde{\nu} f_{v1} \tag{2.15}$$

where

$$f_{v1} = \frac{\chi^3}{\chi^3 + C_{v1}^3} \tag{2.16}$$

where C_{v1} is a constant and χ is given by:

$$\chi = \frac{\tilde{\nu}}{\nu} \tag{2.17}$$

The Production term in the transport equation is modelled by:

$$G_{\tilde{\nu}} = C_{b1}\tilde{S}\tilde{\nu} \tag{2.18}$$

where:

$$\tilde{S} = S + \frac{\tilde{\nu}}{\kappa^2 d^2} f_{v2} \tag{2.19}$$

$$f_{v2} = 1 - \frac{\chi}{1 + \chi f_{v1}} \tag{2.20}$$

$$S = \sqrt{\Omega_{ij}\Omega_{ij}} \tag{2.21}$$

Here C_{b1} and κ are constants and d is the distance to the wall. S is a scalar measure of the deformation tensor based on the magnitude of the vorticity, Ω_{ij} is the mean rate of rotation tensor defined by

$$\Omega_{ij} = \frac{1}{2}(\partial_j U_i - \partial_i U_j) \tag{2.22}$$

The destruction term is modelled as

$$Y_{\tilde{\nu}} = C_{w1} f_w (\frac{\tilde{\nu}}{d})^2 \tag{2.23}$$

where

$$f_w = g\Big[\frac{1 + C_{w3}^6}{g^6 + C_{w3}^6}\Big]^{\frac{1}{6}} \tag{2.24}$$

$$g = r + C_{w2}(r^6 - r) \tag{2.25}$$

$$r = \frac{\tilde{\nu}}{\tilde{S}\kappa^2 d^2} \tag{2.26}$$

where C_{w1}, C_{w2} and C_{w3} are constants.

The standard values for the model constants have been used and they are:

$$C_{b1} = 0.1355, \qquad C_{b2} = 0.622, \qquad C_{v1} = 7.1, \qquad \sigma_{\tilde{\nu}} = \frac{2}{3},$$
$$C_{w1} = \frac{C_{b1}}{\kappa^2} + \frac{1 + C_{b2}}{\sigma_{\tilde{\nu}}}, \qquad C_{w2} = 0.3, \qquad C_{w3} = 2.0, \qquad \kappa = 0.4187$$

Note that as the turbulence kinetic energy is not computed in this model, the term containing it in the eddy-viscosity hypothesis 2.9 is absorbed into the pressure term and one is really solving for a modified pressure field.

The wall boundary condition for the modified turbulent viscosity is $\tilde{\nu} = 0$.

The $\overline{v^2} - f$ model

The $\overline{v^2} - f$ model [9] is a 4-equation eddy viscosity type model. It is based on the $k - \varepsilon$ model, but is modified to account for near wall anisotropy. It uses the transport equations for k and ε developed in section 2.5.1. The formulation of the eddy viscosity is however not the same. To model the eddy-viscosity the model solves a transport equation for a wall normal velocity scalar $\overline{v^2}$, and an elliptic equation for a redistributive term f. The version of the $v^2 - f$ model implemented has been modified for numerical stability [10], and takes the following form:

$$\partial_t \overline{v^2} + U_j \partial_j \overline{v^2} = kf - 6\frac{\overline{v^2}}{k} + \partial_j(\nu_T \partial_j \overline{v^2}) + \nu \partial_j \partial_j \overline{v^2} \tag{2.27}$$

$$L^2 \partial_j \partial_j f - f = \frac{C_1}{T}(\frac{\overline{v^2}}{k} - \frac{2}{3}) - C_2 \frac{\mathbb{P}}{k} \tag{2.28}$$

Where L is a turbulent length scale given by:

$$L = C_L max\Big(\frac{k^{\frac{3}{2}}}{\varepsilon}, C_\eta \frac{\nu^{\frac{3}{4}}}{\varepsilon^{\frac{1}{4}}}\Big) \tag{2.29}$$

The eddy viscosity is computed according to:

$$\nu_T = C_\mu \overline{v^2} T \tag{2.30}$$

Where T is the turbulent time scale

$$T = max\Big(\frac{k}{\varepsilon}, 6\sqrt{\frac{\nu}{\varepsilon}}\Big) \tag{2.31}$$

The model constants used are:

$$C_\mu = 0.22, \qquad C_\eta = 70, \qquad C_{\varepsilon 1} = 1.44, \qquad C_{\varepsilon 1} = 1.92,$$
$$C_1 = 1.4, \qquad C_2 = 0.3, \qquad C_L = 0.23, \qquad \sigma_k = 1, \qquad \sigma_\varepsilon = 1.3$$

The wall boundary conditions for this model are:

$$u_i = k = \overline{v^2} = f = 0$$

$$\varepsilon = 2\nu\Big(\frac{k}{y_p^2}\Big)$$

where y_p is the distance from the cell centre to the wall.

For more information on the $v^2 - f$ model consult [6] and for details of this specific implementation consult [11]

The Reynolds Stress Model

The Reynolds stress model considered in this paper is the Low-Reynolds number Stress-Omega model, it solves an additional 7 equations in order to close the RANS equations. The equations solved are the 6 equations for the Reynolds stresses from the RSTE (2.6) and an equation for ω, an inverse turbulent timescale. This additional equation is solved in order to help close the 6 equations for the Reynolds stresses.

The transport equation for ω is modelled as follows:

$$\partial_t \omega + U_j \partial_j \omega = G_\omega + \nu \partial_j \partial_j \omega + \partial_j(\frac{\nu_T}{\sigma_\omega} \partial_j \omega) - Y_\omega \tag{2.32}$$

where ν_T is turbulent kinematic viscosity, σ_ω is a model constant, G_ω is the production and Y_ω is the destruction of ω. The turbulent kinematic viscosity is modelled by:

$$\nu_T = \alpha^* \frac{k}{\omega} \tag{2.33}$$

where α^* is a low Reynolds number correction factor given by:

$$\alpha^* = \alpha^*_\infty \Big(\frac{\alpha^*_0 + \frac{Re_t}{R_k}}{1 + \frac{Re_t}{R_k}} \Big) \tag{2.34}$$

here α^*_∞, α^*_0 and R_k are model constants whilst $Re_t = \frac{k}{\nu\omega}$ is the turbulent Reynolds number.

The production of ω is modelled as:

$$G_\omega = \alpha_\infty \Big(\frac{\alpha_0 + \frac{Re_t}{R_\omega}}{1 + \frac{Re_t}{R_\omega}} \Big) S_{ij} S_{ij} \tag{2.35}$$

where α_∞, α_0 and R_ω are model constants.

The destruction is given by the following expression:

$$Y_\omega = \beta f_B \omega^2 \tag{2.36}$$

where β is a model constant and f_B is given by:

$$f_B = \frac{1 + 70\chi_\omega}{1 + 80\chi_\omega} \tag{2.37}$$

and

$$\chi_\omega = \Big| \frac{\Omega_{ij}\Omega_{jk}S_{ki}}{(\beta^*_\infty \omega)^3} \Big| \tag{2.38}$$

where β^*_∞ is a model constant. The standard values of the model constants for the ω transport equation are:

$$\alpha^*_\infty = 1, \qquad \alpha_\infty = 0.52, \qquad \alpha_0 = \frac{1}{9}, \qquad \alpha^*_0 = \frac{\beta}{3},$$
$$\beta^*_\infty = 0.09, \qquad \beta = 0.072, \qquad R_k = 6, \qquad R_\omega = 2.95, \qquad \sigma_\omega = 2$$

The wall boundary condition for ω is given by:

$$\omega_w = 2500 \frac{(u^*)^2}{\nu}$$

where u^* is the frictional velocity defined in section 2.7.

With this transport equation we are ready to provide the closure model for the Reynolds Stress Transport Equation. The terms that need to be closed are

the turbulent transport d_{ij}^t, the pressure transport d_{ij}^p, the dissipation ε_{ij} and the pressure strain Φ_{ij}.

In this case we model the two transport terms together by a gradient transport model according to the following equation.

$$d_{ij}^t + d_{ij}^p = \partial_l(\frac{\nu_T}{\sigma_k}\partial_l(\overline{u_i u_j})) \tag{2.39}$$

WHere $\sigma_k = 0.82$ is a model constant.

For modelling the dissipation we invoke the assumption of local isotropy and can thus simplify so that we get:

$$\varepsilon_{ij} = \frac{2}{3}\varepsilon\delta_{ij} \tag{2.40}$$

The scalar dissipation rate is in this case determined using ω according to the following equation:

$$\varepsilon = \beta^* f_{\beta*} k\omega \tag{2.41}$$

where

$$\beta^* = \beta_\infty^*\Big(\frac{\frac{4}{15} + (\frac{Re_t}{R_\beta})^4}{1 + (\frac{Re_t}{R_\beta})^4}\Big) \tag{2.42}$$

$$f_{\beta*} = \begin{cases} 1, & if \quad \chi_k \leq 0 \\ \frac{1+680\chi_k^2}{1+400\chi_k^2}, & if \quad \chi_k > 0 \end{cases}$$

and

$$\chi_k = \frac{1}{\omega^3}\partial_j k \partial_j \omega \tag{2.43}$$

where $R_\beta = 8$ is a model constant.

The only thing that remains now is to model the pressure strain. In this case it is accomplished in the following way:

$$\begin{aligned}\Phi_{ij} = -(C_1\varepsilon + C_1^* P)b_{ij}) + C_2\varepsilon(b_{ik}b_{kj} - \frac{1}{3}b_{mn}b_{mn}\delta_{ij}) + (C_3 - C_3^*\sqrt{b_{mn}b_{mn}})kS_{ij} \\ + C_4 k(b_{ik}S_{jk} + b_{jk}S_{ik} - \frac{2}{3}b_{mn}b_{mn}\delta_{ij} + C_5 k(b_{ik}\Omega_{jk} + b_{jk}\Omega_{ik})\end{aligned} \tag{2.44}$$

where b_{ij} is the Reynolds anisotropy tensor defined as:

$$b_{ij} = \frac{\overline{u_i u_j}}{k} - \frac{2}{3}\delta_{ij} \tag{2.45}$$

The model constants are:

$$\begin{aligned} C_1 = 3.4, \qquad C_1^* = 1.8, \qquad C_2 = 4.2, \qquad C_3 = 0.8, \\ C_3^* = 1.3, \qquad C_4 = 1.25, \qquad C_5 = 0.4 \end{aligned}$$

2.6 Large Eddy Simulation

A computationally more demanding alternative to the RANS approach to turbulence modelling is Large Eddy Simulation(LES). In a LES, the dynamics of the larger scale motions, or eddies, are computed explicitly whilst the smaller scale motions are modelled. The rationale behind this is that quantities such as momentum, mass, energy and passive scalars are mostly transported by the large eddies. Additionally, the large scale eddies are more problem dependent, as they are dictated by the geometry and boundary conditions involved, whilst the small eddies can be assumed to have a more universal character and thus the chance of finding a universal model for these are higher.

The development of an LES model consists of 3 steps:

- A filtering operation is defined to decompose the velocity into a resolved component and a residual component.
- The equations for the evolution of the filtered velocity field are derived from the Navier-Stokes and continuity equations. This equation contains unclosed terms comprising the a priori unknown residual components.
- Closure is obtained by modelling the unclosed term in the above equation by known quantities.

2.6.1 Filtering

The first step on the way is to define a filtering operation. This filtering process removes the smaller scale fluctuations. For a function F the general form of such a filter can be written as

$$\langle F(x,t)\rangle = \int G(r,x)F(r,t)dr \tag{2.46}$$

where $\langle F\rangle$ is the filtered variable, G is the specified filter and the integration is over the entire domain.

In the current application in which the finite volume method is used(see section 3.2), this implicitly provides a filtering function according to:

$$G(r,x) = \begin{cases} \frac{1}{V}, & if \quad r \in C \\ 0, & otherwise \end{cases}$$

where C is the computational cell containing x and V is the volume of that cell. We can then simplify the filtering to only include the computational cell which leaves

$$\hat{F}(x,t) = \frac{1}{V}\int_C F(r,t)dr \tag{2.47}$$

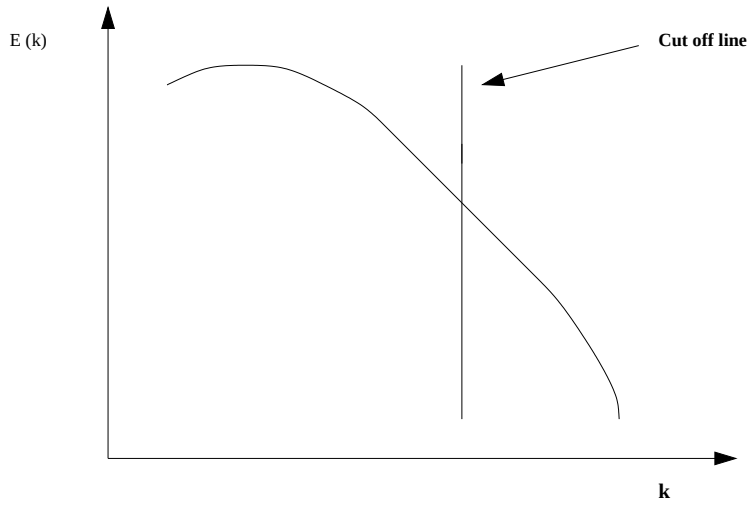

Figure 2.3: Illustration of the filtering operation. E(k) is the energy contained in the motions of wavenumber k. With the filter all the motions of wavenumber greater than the cut of line are filtered out whilst those with a smaller are solved explicitly

The residual field is now defined as

$$f'(x,t) = F(x,t) - \langle F(x,t) \rangle \tag{2.48}$$

This seems very similar to the Reynolds decomposition. There are however significant differences. One important difference, is that $\langle F \rangle$ is an instantaneous velocity, not a statistic. Another is that, in general, $\overline{f'(x,t)} \neq 0$ which means that if we gather statistics to generate a mean flow field this will not nessecarily converge towards the actual mean flow field.

It is usually assumed that filtering and differentiation commute. This assumtion is implicitly invoked when deriving the filtered Navier-Stokes equations in the majority of cases. It should be noted that this assumption is only valid if $G = constant$. In this case this criterion is not fulfilled. The error induced by this assumtion is however thought to be within the inaccuracy of the closure model.

2.6.2 Filtered Navier-Stokes

If we now employ this filtering operation on the incompressible Navier-Stokes equations in a rotating frame of reference we obtain:

$$\partial_t \langle \tilde{u_i} \rangle + \langle \tilde{u_j} \rangle \partial_j \langle \tilde{u_i} \rangle = -\frac{1}{\rho} \partial_i \langle \tilde{p} \rangle + \nu \partial_j \partial_j \langle \tilde{u_i} \rangle - (\Omega_j r_j \Omega_i - \Omega_j \Omega_j r_i) - 2\Omega_l \langle \tilde{u_k} \rangle \epsilon_{lki} - \partial_j \tau^r_{ij} \tag{2.49}$$

$$\partial_j \langle \tilde{u_i} \rangle = 0 \tag{2.50}$$

where τ_{ij}^r is the residual stress tensor. It is a result of applying the filtering to the nonlinear term, and the fact that the filtering of a product is not equal to the product of the filtered fields. It takes the following form

$$\tau_{ij}^r = \langle \tilde{u_i} \tilde{u_j} \rangle - \langle \tilde{u_i} \rangle \langle \tilde{u_j} \rangle \tag{2.51}$$

The residual stress tensor plays an analogous role to the Reynolds stresses tensor. It contains the unknown correlation $\langle \tilde{u_i} \tilde{u_j} \rangle$, which means that the set of equations is unclosed and some sort of closure relation is required.

2.6.3 The closure relation

The closure model used in this project is the Dynamic Smagorinsky-Lilly model.

By analogy with the Reynolds stresses it seek to model the residual stresses using the eddy-viscosity hypothesis. In terms of filtered variables this can be expressed as

$$\tau_{ij}^r = \frac{2}{3} k_r - 2\nu_T \langle S_{ij} \rangle \tag{2.52}$$

where $k_r = \frac{1}{2}\tau_{ii}^r$ is the residual kinetic energy and $\langle S_{ij} \rangle$ is the filtered rate of strain given, which is defined as:

$$\langle S_{ij} \rangle = \frac{1}{2}(\partial_j \langle \tilde{u_i} \rangle + \partial_i \langle \tilde{u_j} \rangle) \tag{2.53}$$

Now, by analogy with the mixing length model, the eddy viscosity is modelled as:

$$\nu_T = L_s^2 \langle S \rangle \tag{2.54}$$

Where L_s is a length scale and $\langle S \rangle = \sqrt{2 \langle S_{ij} \rangle \langle S_{ij} \rangle}$ is the characteristic filtered rate of strain. The length scale is given by

$$L_s = min(\kappa d, C_s V^{\frac{1}{3}}) \tag{2.55}$$

Here κ is the von Karman constant,d is the distance to the closest wall and V is the volume of the computational cell. In the Smagorinsky-Lilly model, the Smagorinsky constant C_s is indeed constant. In the dynamic model considered here,C_s is a variable computed based on the resolved flow field variables. The details of whitch can be found in [12].

This type of closure model is not unproblematic however. For as we can see the filtering operation is not included in the formulation. This means that the equations solved is independent of the type of filter one is suposedly using. The filtering operation thus only has conceptual value. Furthermore, as the size of the computational cell is included the solution is entirely mesh dependent! It is however believed that if the mesh resolution is sufficient the solution will become mesh independent. The reason for this is that as the cell size is decreased the

modification of the Navier-Stokes equations diminishes. If the mesh is fine enough to resolve all motions down to the Kolmogorov scales, the LES is in fact a Direct Numerical Simulation(DNS) and ,provided that the numerics is good enough, it is an exact solution to the Navier-Stokes equations.

It is important to note that as we are solving for instantaneous fields a good evaluation of the mean flow field requires us to collect statistics. To obtain a statistically valid flow field we must run the LES for a significant amount of time. In this case we have collected data for 60 seconds, for time steps of 0.1seconds. This is probably too short of a time but it should still display close to the behaviour of the true mean.

2.7 Wall treatment

It should be needless to say that turbulent flows are significantly affected by the presence of walls. Somewhat surprisingly however is the fact that given the proper length and velocity scalings there seems to be a universal behaviour for the flow in the near wall region. This scaling is given by:

$$y_+ = \frac{yu_*}{\nu}$$

$$U_+ = \frac{U}{u_*}$$

where y is the wall normal distance, U is the mean tangential velocity and u_* is the frictional velocity given by:

$$\rho u_*^2 = \tau_w$$

where τ_w is the wall friction.

Given this scaling the velocity close to the wall can generally be split into three parts. The linear sub layer, the buffer region and the logarithmic layer(see Figure 2.4.

The inner most region, is called the linear sublayer. It is located at approximately $0 < y_+ < 5$. In this layer the viscous forces dominate. Here the velocity increases linearly according to

$$U_+ \simeq y+$$

A little further out in the approximate region of $30 < y_+ < 250$ we have the logarithmic layer. In it there is a balance between viscous forces and inertial forces. The resulting velocity profile is:

$$U_+ = \frac{1}{\kappa} ln(y_+) + A$$

where κ and A are constants.

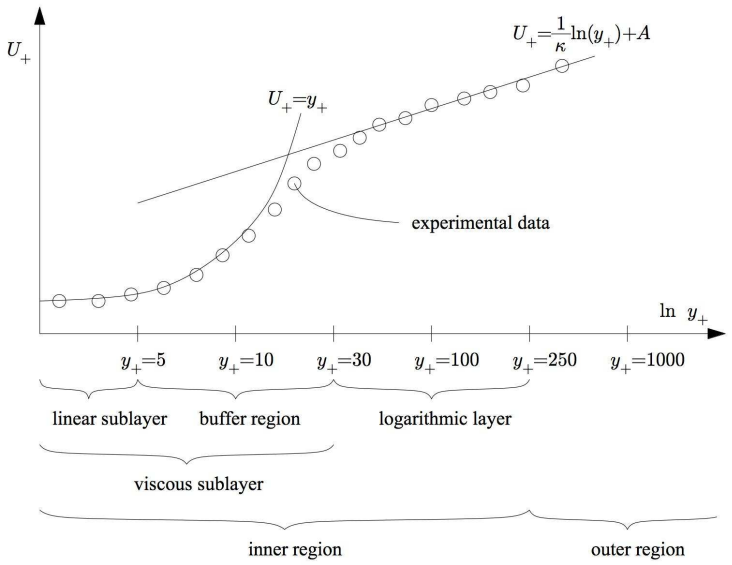

Figure 2.4: A schematic overview of the different layers in wall bounded turbulent flow.

Between these two regions is a buffer region, an approximation to the velocity profile in this region can be found by matching the solutions of the linear sublayer and the logarithmic layer.

Outside the logarithmic layer we found the fully turbulent region, which is "unaffected" by the wall.

For the LES this dampening of velocities towards the wall has an interesting consequence. It means that the large scale energy containing motions get smaller as we approach the wall. So in order to get an accurate representation of the flow the mesh in the near wall region for the LES must be made finer.

Near wall resolution is not just important for the LES however, as we expect that the flow has largest gradients close to the walls.

A general criterion for achieving a good solution is that the mesh must be fine enough to resolve the laminar sublayer. In this case we expect this to require a very fine mesh as the Ekman Layer is known to have huge gradients whitch means that the y_+ scaling is very fine.

2.8 Particle Transport

The dispersion of aerosols is, in general, a very difficult phenomenon to model. The reasons for this are many, but one of the greatest challenges stems from the fact that the aerosols can affect the flow of the gas in which they are suspended.

Another issue arises from the aerosol-aerosol interactions, which include pro-

cesses such as agglomeration, aerosol break-up, electrostatic forces and so forth. These processes affect the transport of aerosols in a variety of ways that are hard to quantify. For a theory on particle collisions consult [13].

Further complications associated with the evaporation and deposition processes are also to be expected in most cases.

In this project, we assume that the concentration of aerosols is low enough that they can be treated as passive in the transport process. This means that the aerosols do not affect the dynamics of the flow of air that carries them. This alows us to use the 'a priori' determined velocity fields in the computations of the aerosol transport.

Furthermore, as the concentration of aerosols is assumed to be low, we will assume that the effects of particle interactions also are negligible.

A simplified model for deposition and evaporation will also be used, so that any aerosol that comes into contact with a wall will be considered to be deposited, and no secondary evaporation will be allowed.

The aerosols considered in this project are spherical water dropplets ranging in diameter from $1\mu m$ to $20\mu m$.

2.8.1 Discrete particle approach

One way to model the transport of aerosols is to consider the force balance on individual particles and use this to determine the path of the particle within the domain. Using the assumtions stated above, the force balance can be expressed in a Lagrangian frame of reference as

$$\frac{du_{p_i}}{dt} = F_D(u_i - u_{p_i}) + \frac{g_i(\rho_p - \rho)}{\rho_p} + \frac{1}{2}\frac{\rho}{\rho_p}\frac{d}{dt}(u_i - u_{p_i}) + \frac{\rho}{\rho_p}u_{p_i}\partial_i u \tag{2.56}$$

where u_p is the velocity of the particle, F_D) is the drag force coefficient per unit mass, u is the carrying fluid velocity, g is the gravitational acceleration, ρ and ρ_p are the densities of the fluid and the particle. Brownian forces and Saffman's Lift Forces are assumed to be negligible.

Here F_D is given by

$$F_D = \frac{18\mu}{C_c\rho_p d_p^2} \tag{2.57}$$

where d_p is the diameter of the particle and C_c is the Cunningham correction factor given as

$$C_c = 1 + \frac{2\lambda}{d_p}(1.257 + 0.4e^{-(1.1d_p/2\lambda)}) \tag{2.58}$$

where λ is the molecular mean free path. For the conditions being simulated the Cunningham correction factor is significant for submicron particles only.

This approach is very advantageous if we are interested in the rate of depostion, as it is easy to determine wheter or not a particle has come into contact with the wall.

Note that if we are dealing with mean flow fields, such as in the RANS case, these equations do not account for the effect of turbulent fluctuations.

2.8.2 Scalar field approach

An alternative way to to approach the transport of the aerosols is to model the concentration of the aerosols as a passive scalar field. The evolution of such a scalar field is governed by the convection-diffusion equation.

$$\partial_t \tilde{c} + \tilde{u} j \partial_j \tilde{c} = \gamma \partial_j \partial_j \tilde{c} \tag{2.59}$$

As in the case of the velocity field we can arrive at a Reynolds averaged equation for the concentration of the scalar. We simply insert the Reynolds decomposition $\tilde{c} = C + c$ along with the decomposition of the velocity and take the ensemble average. This results in the following equation:

$$\underbrace{\partial_t C + U_j \partial_j C}_{\text{Total rate of change}} = \underbrace{\gamma \nabla^2 C}_{\substack{\text{molecular} \\ \text{diffusion}}} - \underbrace{\partial_j \overline{u_i c}}_{\text{scalar flux}}$$

Here the scalar flux, which is the result of averaging the nonlinear advective term, is unknown, and needs to be modelled in some way in order to close the equations.

In this project this option was considered and even attempted, but as our primary data source is of the deposition rate, it was found that it yielded little relevant information when compared to the discrete approach, and so the results have not been included.

Chapter 3

Numerical Simulations

3.1 Fluent 6.3

To simulate the different models mentioned above the comercially available Computational Fluid Dynamics(CFD) package ANSYS Fluent 6.3 has been used. Of the models considered herin all but the $\overline{v^2} - f$ model are already implemented in the standard version of Fluent. The $\overline{v^2} - f$ model has been implemented in fluent using the User Defined Scalars(UDs) routine. The required code for this had been provided.

3.2 The finite volume method

Fluent employs the finite volume method to solve the partial differential equations as algebraic equations. This is the most commonly used method in CFD. and it consists of 3 steps.

1. The Geometry is divided into several discrete control volumes, called computational cells, in what we call a computational mesh.

2. Then the governing equations are integrated over individual control volumes to obtain algebraic equations for the discrete dependent variables(i.e. velocity, pressure, etc). Which are located at the center of the cell.

3. The equations are linearised to obtain a linear system of equations that can be readily solved on a computer.

The issues concerning the generation of a computational mesh is discussed in section 3.3. The rest of the proceedure is illustrated here for the case of general mass conservation.

On integral form the equation of mass conservation reads:

$$\oint \rho \tilde{u} \cdot dA = 0 \tag{3.1}$$

Where A is the surface of the control volume. Integration over an entire computational cell yields:

$$\sum_{f}^{N_{faces}} J_f A_f = 0 \tag{3.2}$$

where $J_f = \rho u_n$ is the mass flux through face f.(Here u_n is the velocity normal to the face f). In order to proceed further, it is nesecarry to relate u_n to the stored values of $\tilde{u}$ at the centers of the cells. Usually, the values at cell faces are obtained by linear interpolation between the cell centers. This does however yield an unphysical checker-boarding effect on the pressure, ans so a momentum-weighted averaging proceedure is used instead. The details of this proceedure can be found in [14].

When solving a problem with the finite volume method, the solution is obtained iteratively. This means that system of equations must be solved several times using the most recently obtained solution to calculate the next. As the first iteration also requires a previous solution to start the calculations. This initial 'guess' needs to be provided in order to start the calculations.

Whether a convergent solution is obtained and the number of iterations required to obtain it depends both on the numerical schemes involved and on the initial guess of the flow field. The numerical schemes used in this project is found in Section 3.4. A discussion on convergence is found in Section3.5.

3.3 Computational Mesh

A vital part of using the finite volume method is the generation of a computational mesh. The process, called meshing, consists of splitting the geometry into many small computational cells. This can, of course, be accomplished in any number of ways, but very few of these configurations are suitable for use. In fact, in many CFD simulations the convergence of the simulations is strongly dependent on the quality of the mesh. Furthermore, even if the solution converges, the quality of that solution will depend upon the mesh.

One of the most important factors one has to consider when creating the mesh is the size of the cells. Small cells do, in general, give a higher quality solution, but they come at the cost of computational expense. In the case of CFD the mesh must be fine enough to capture all the relevant effects of the flow. To determine which effects are present and relevant is difficult, but some insight into fluid mechanics can help us along the way. For Fluent to properly resolve the viscous sublayer, the centers of the cells closest to the walls must be located within $y_+ = 1$. This criterion is easily met by the meshes used here. A fine enough mesh is however not a sufficient criterion, one must also consider the quality of each cell, and their placement in relation to eachother. Among other

things it is important that the elements are well shaped(little skewness) and that adjecent elements have similar volumes.

3.3.1 RANS case

If we assume the effect of gravity on the airflow to be negligible the problem inside the chamber reduces to an axisymmetric case. For the RANS approach we can thus employ a 2-dimensional mesh of a plane that contains the cyllinder axis, further we can uses symmetry to cut the computational domain in half with the axis of rotation. The remaining region is a square 2 feet by 3 feet (see figure 3.1) which has been meshed with 200 000 quadratic elements. Boundary layer meshes have been applied to all three edges that represent walls. This grid is extremely fine, but previous trials have shown that the solution is very grid sensitive. This is probably due to the formation of Ekman Layers along the disk shaped walls. The present resolution is believed to be sufficent in order to achieve a grid independent solution.

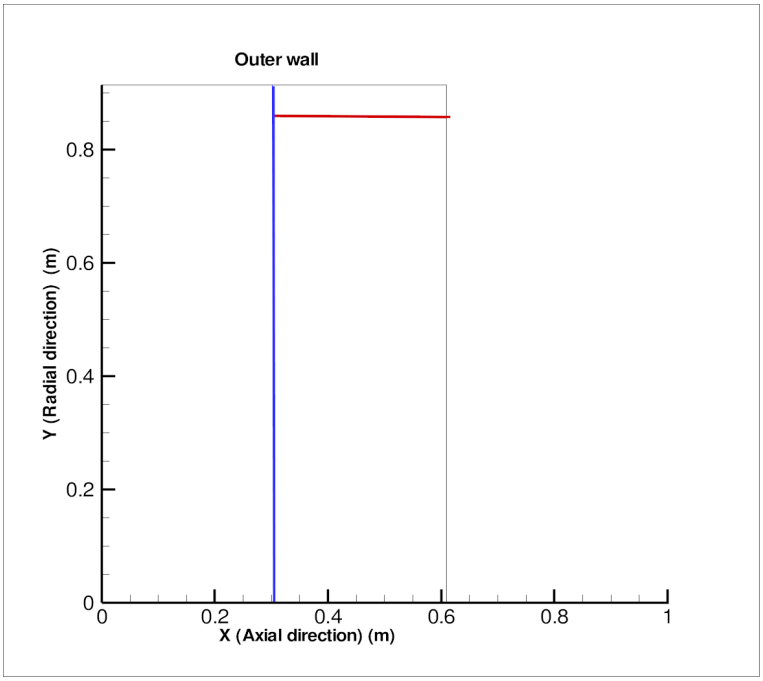

Figure 3.1: The computational domain. The x-axis is the axis of rotation, the vertical line in the interior is the center of the domain and the horizontal line is located at y=0.85 and is used for comparing the results of different models.

The computational domain could be further cut in half by the symmetry axis at the center of the domain. This has not been done, in order to simplify

the process of obtaining the three dimensional flow field will be requird for the particle transport.

3.3.2 LES case

In the LES we cannot use the simplification to a two dimenisonal case. The reason for this is that the filtered equations are fluctuating fields, and so the assumption of axisymmetry is not valid at any single temporal step. The resulting mean fields should however be axisymmetric. In this case we must thus use a full 3-dimensional mesh of the aerosol chamber. The mesh used contains approximately 12 million cells and, as in the RANS case, boundary layer meshes have been applied to the walls. This is a very fine mesh, but part of the purpose of conducting a LES was to provide a reliable data set, and for this kind of wall bounded flow an extremly fine mesh is required. In terms of Kolmogorov scales the spatial resolution is in the range $0.6 - 1.1$ and the temporal resolution is approximately 1.6(these are of course computed a posteriori). The belief that the LES will provide a reliable data set thus seems likely. One approximation has however been made, the circular shape of the outer wall is approximated by a polygon, which results in a slightly dented cylinder. The effect of this on the mean flow field is thought to be minimal. A part of the LES mesh is depicted in Figure 3.2.

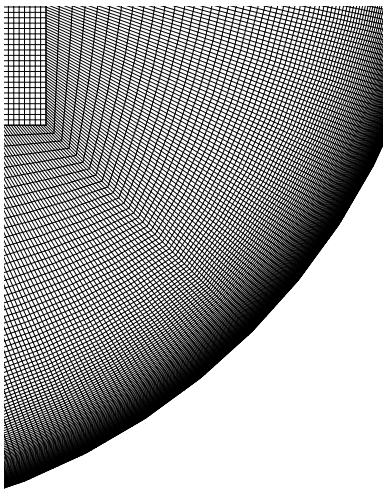

Figure 3.2: A part of the grid used for LES

3.4 Solver options

For all the simulations conducted in this project Fluents pressure based segragated algorithm has been used. In the seggregated algorithm the coupled governing equatons for the flow variables are solved sequentially in a decoupled manner in each iteration. This approach requires more iterations in order to obtain a convergent solution, but it has the advantage of requiring less memory than a coupled approach.

For the RANS simulations the Third-order MUSCL discretization was used for all variables except the pressure for which the PRESTO scemes was used.

For the LES the bounded central difference scheme was used for the velocity variables along with the second order implicit temporal discretization and the standard pressure interpolation scheme. For more information about the various discretization schemes consult [14].

For the discrete particle simulation a step length factor of 5 was used, and the Cunningham correction factor is set to 1 as we are dealing with particles in the μm range.

3.5 Convergence

The correct solution to the equations posed in a CFD problem is seldom know. Therefore, it is not possible to accuratley predict the numerical error in the computations. Several methods for estimating the size of the error do however exist. One of these is the residual. The residual says something about the imbalance in quantities that should be equal for the equations to be solved correctly. A small difference implies that the solution is close to convergence. We say that a solution is converged if the residuals are low and do not change between consecutive iterations we say that the solution is converged. It is however not nescessarily true that the solution is converged to the correct solution. To determine this often requires physical interpretation.

As a convergence criterion for the models in this paper I demanded that the residual of all the variables for whitch equations are solved for as well as that of continuity is stable and small. Additionally , for the RANS case, I have required that the sum of he forces on the cyllinder in the axial direction must be low and stable. This additional requirement is based on physical reasoning and a true solution of the equations should display this characteristic. For definitions of the individual residuals consult [14].

Chapter 4

Results

4.1 Fluid Flow

As there exists no reference data for the flow field inside the chamber the LES data is considered to be the primary result. The reason for this choice is that, according to the discussion in Section 2.6 and Section 3.3.2, it is believed to be the most reliable data set. For this reason the results section for the fluid flow has been divided into two section. In the first the predictions of the LES model is discussed to determine the features of the flow field. In the second the LES data is compared to the RANS models to determine their predictive capabilities. To this end the majority of the plots for the LES model are taken from a region whitch is identical to the one modelled in the RANS approach(see figure 3.1. If not stated otherwise, the contour plots will refer to such a region and the line plots will be according to the lines defined in this domain. This should however not be a misrepresentation of the LES data as the problem indeed is axisymmetric.

4.1.1 LES results

To begin the description of the LES flow let us first consider the contour plot of mean velocity magnitude in figure 4.1(a). Here it can be observed that Ekman boudary layers have indeed formed along the disk shaped walls, apart from that there appears to be very little variation in the mean velocity in the axial direction. This state in which the velocity is not a function of the direction along the rotational axis is sometimes referred to as the Taylor-Proudman limit. We can also see that a boundary layer has formed near the outer wall. Furthermore, it is apparent that there is a considerable region in the center of the chamber with relativly low velocity.

As there is little variation in the mean velocities in the axial direction, I will use the velocity profile at the center of the plane , located at $x = 0.3048$, to classify the variations in the mean circumferential velocity as a function of radial distance (Y). The plot can be found in figure 4.2(a), and it reveals a clearly

turbulent velocity profile. This is determined easily, because in the laminar case, the velocity profile would have been linear. Furthermore, the fact that the slope of the plot increases with radial distance seems to indicate that the turbulence level should follow this trend as well.

The contour plot of the Root Mean Square(RMS) velocity in figure 4.1(c) reveals that the there is a general increase in velocity fluctuations in the radial distance up to about $y = 0.75$ and then it receeds again towards the wall. This is rather unexpected, and difficult to explain. It is believd to be caused by a phenomenon referred to as "inactive motion" [15], an inviscid instability process that creates strong anisotropic turbulent fluctuations. That the turbulent fluctuations are highly anisotrpic can be concluded from Figure 4.2(d). If not for this effect we would have expect the turbulence to be at its maximum at the boundary layer close to the outer wall as the gradient of the velocity is greatest here. Furthermore, there appears to be little axial variation apart from the Ekman boundary layers. The effect of the Ekman layers, are to increase the fluctuations, except close to the axis where they appear to diminish them. To explain this effect it is easiest to consider the problem in terms of the production of turbulence kinetic energy

$$P = -\overline{u_i u_j}\partial_j U_i$$

In most of the Ekman Layer the gradient in the axial direction dominates. Furthermore, the velocity component in the circumferential direction is dominant which means that the production by the Ekman layer can be approximated by

$$P^e \approx -\overline{u_\theta u_x}\partial_x U_\theta$$

Since the thickness of the Ekman layer is as good as uniform the magnitude of $\partial_x U_\theta$, in the Ekman layer as a function of radial distance, can be determined from the figure 4.2(a) as the deviation of the velocity profile from the linear profile. A plot of this can be found in figure 4.2(c). If we compare this to the plot of RMS velocity 4.1(c), we see that the maximum shear and the maximum of the fluctuations are not located at the same radial distance. This means that there must be a radial variation in the correlation $\overline{u_\theta u_x}$. The production of $\overline{u_\theta u_x}$ is given by

$$P_{\theta x} = -\overline{u_x u_x}\partial_x U_\theta - \overline{u_x u_r}\partial_r U_\theta - \overline{u_\theta u_x}\partial_x U_x - \overline{u_\theta u_r}\partial_r U_x$$

As stated earlier the circumferential velocity component dominates. This yields:

$$P_{\theta x} \approx -\overline{u_x u_x}\partial_x U_\theta - \overline{u_x u_r}\partial_r U_\theta$$

The second component in the equation is dependent on the radial position approximately according to the gradient in figure 4.2(a). This term is increasing with radial distance. The resulting production by the Ekman Layer is thus depenedent on both the velocity gradient in the circumferential direction and on

the deviation of the velocity in the circumferential direction from the laminar profile.

A feature of great importance when one is concerned with particle transport is the mean secondary flow field. The reason for this is that the mean secondary flow describes the motion of the flow in the axial and radial directions and so they are of vital importance in the transport of particles towards the walls. The mean secondary flow can be described by a stream function, since the mean flow is independent of the circumferential direction. This stream function is depicted in figure 4.1(b) and it tells us that the secondary flow consists of two counter rotating vortices located close to each of the disk shaped walls. The secondary flow is quite weak. It is at least one order of magnitude smaller than the circumferential velocity everywhere except close to the rotational axis, and compared to the maximum circumferential velocity it is always less than 8%. This means that there is little advection in the $r - x$ plane. This has interesting consequences. It implies that the local rate of production of turbulence should be dominant when determining the turbulence at a given point.

To illustrate the turbulent fluctuations that are present in the flow, let us consider the instantaneous axial velocity in three axial cuts of the cyllinder located 5cm, 10cm and 15cm from the one of the disk shaped walls. These cuts are depicted in figure 4.3(b),(c)and (d). If we consider the three marked structures in each Figure it is clear that they represent three structures with dimesnisons of at least 10cm in the axial directions. These turbulent structures are large and very energetic. They play an important role in any transport process within the chamber, and are not a feature of the mean flow field.

4.1.2 Comparison of RANS and LES

In this section the results of the LES and the three RANS models that were considered are compared. One characteristic that was similar for all the models where that there was little axial variation in the circumferential velocity except close to the disk shaped walls where all the models predicted Ekman boundary layers of similar thickness. This can be seen in Figure 4.4.

Figure 4.4 also reveals that there are significant differences in the predicted circumferential velocities of the models. The plot of circumferential velocity, at the center of the chamber, as a function of radial distance(Y) in figure 4.5 reveals the nature of these differences. From it we can see that both the eddy-viscosity models predict nearly linear velocity with a slight boundary layer near the outer wall. The boundary layer of the SA model seems to agree quite well with that of the LES, whilst the $v^2 - f$ model predicts a slightly less pronounced one of approximately the same thickness. The RSM model on the other hand predicts an entirely different velocity profile. It has a much more pronounced boundary layer at the outer wall and close to the axis it has a region in whitch the change of circumferential velocity actually decreases with radial distance. This is a strange

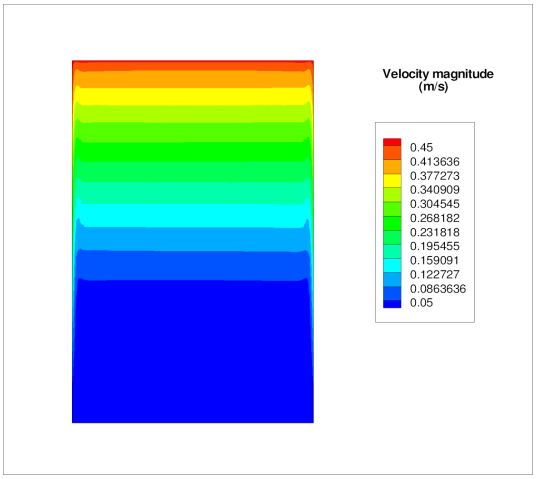

(a) Contours of mean velocity magnitude

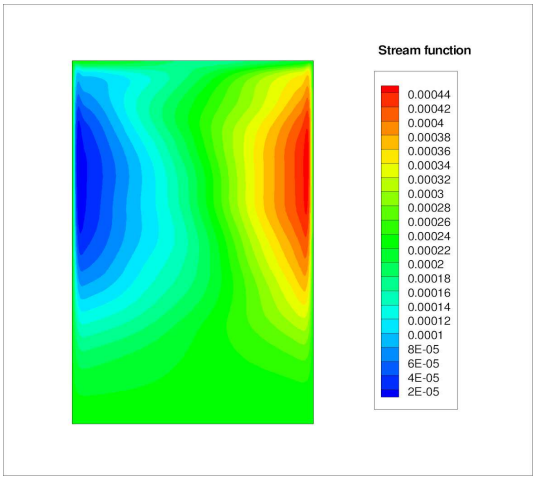

(b) Cotours of mean stream function

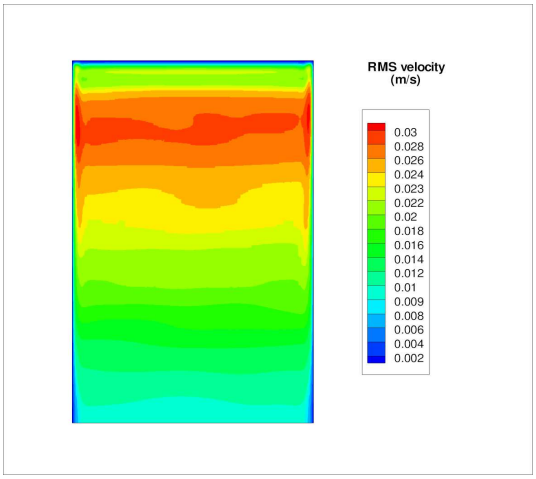

(c) Cotours of RMS velocity magnitude

Figure 4.1: Contours of LES mean flow variables for $z = 0$ and $y \geq 0$

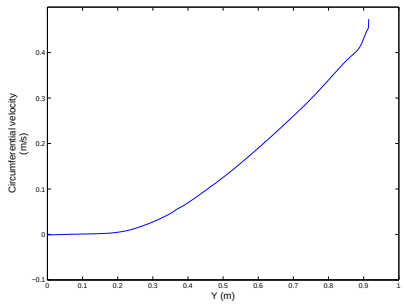

(a) Mean circumferential velocity

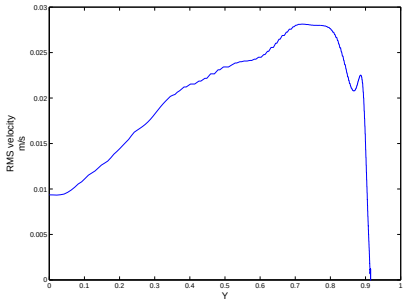

(b) RMS velocity magnitude

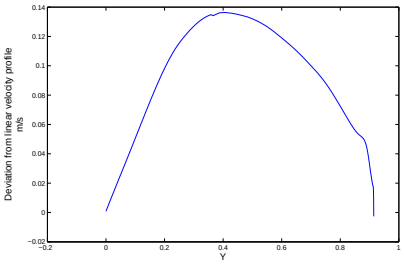

(c) Deviation of the mean circumferential velocity from a linear profile

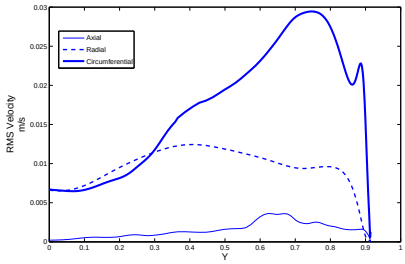

(d) Componential RMS velocity

Figure 4.2: Plot of LES data at $x = 0.3048$ and $z = 0$

effect that is a common issue with this type of model.

If we consider the secondary flow patterns revealed by the stream functions in figure 4.6 we see that all the RANS models predict the same holistic nature of the secondary flow as the LES. There are however slight differences. For instance, in all the RANS models the vortices are centered significantly closer to the outer wall. Furthermore, the shapes of the vortices are different in all the models. The magnitudes of the secondary flows also differ. One way to measure the secondary flow is to look at the ratio of the maximum secondary flow magnitude to that of the maximum velocity magnitude. If we denote this ratio by R this can be expressed as:

$$R = max\left(\sqrt{U_x^2 + U_r^2}/|U_{max}|\right)$$

where U_max denotes the maximum velocity in the domain. The values of R for the different models are found in table 4.1. These show that the two eddy viscosity models predict a significantly lower magnitude than the RSM and the LES. This is an indication that the generation mechanism for the mean secondary flow is caused partially by turbulence anisotropy. The strength of the secondary flow field is likely to be very important when determining the transport of aerosols.

A very significant difference between the LES and all the RANS models can be observed by considering Figure 4.1(c) of the RMS velocity and Figure 4.7 of

Table 4.1: Ratio of maximum secondary flow magnitude to maximal flow magnitude (R)

Model	R
LES	0.08
RSM	0.0706
SA	0.0306
$v^2 - f$	0.0109

the Turbulent viscosity ratio ν_T/ν for the RANS models(this is not a primary result of the RSM model). As we know, the LES predicts increasing turbulence level with radial distance up to $y \approx 0.75$. The trend for the RANS models is however to predict the highest turbulence levels in the center of the chamber and decreasing levels towards the outer walls. This seems to be unphysical as we know that turbulence is mainly produced close to the walls. This is however a common defect in RANS models when applied to low Reynolds number flows. The reason for the issue is best described by considering the limiting case of laminar flow.

In a laminar flow we of course consider the turbulence kinetic energy to be zero.

$$k = 0$$

If we consider the ratio of turbulent time scale to laminar time scale, the laminar case would imply that the ratio approaches infinity. This is expressed:

$$\frac{Sk}{\varepsilon} \to \infty$$

Thus, in a low reynolds number turbulent flow we must expect that:

$$k << 1 \qquad \frac{k}{\varepsilon} >> 1$$

This does however present a problem as we know the eddy-viscosity scales as:

$$\nu_T \sim \frac{k^2}{\varepsilon} = k(\frac{k}{\varepsilon})$$

Thus we have no way of determining the actual value of the eddy-viscosity in this case. Ideally the models should predict zero eddy viscosity in the laminar case. A very low prediction in the center of the chamber would thus seem intuitively correct. The plots in figure 4.7 reveals that this is unforunately not what the models predict.

The issue of whether the eddy-viscosity is a suitable way to determine the turbulence levels for the RSM model could be raised. If we instead consider the turbulence kinetic energy for the RSM model(see Figure 4.8) we see that it displays the same character as those of the eddy-viscosity. The reason behind

this is similar to the one explained above, and will not be considered in detail here.

From Figure 4.7 and 4.8 it is also apparent that the turbulence levels predicted by the different models varies significantly.

The results of this section clearly shows that there are significant differences in the predictive capabilities of the RANS models, and none of them faithfully predicted all the flow characteristics displayed by the LES solution. The difficulty of modelling this low Reynolds number rotationally driven wall bounded flow has thus clearly been demonstrated.

4.2 Particle Transport

The simulations of aerosol transport consisted of two parts.

Firstly, the axisymmetric case of the RANS models was used as a preliminary study to determine the approximate size of an aerosols that could be suspended in the air.This simulation consisted of releasing water droplets ranging in size from 1 to $20\mu m$ from close to the centre of the chamber. The result was that all particles of diameter greater than approximately $7\mu m$ deposited on the wall after approximately 10^3 seconds for both the RSM and the SA model. The particles of size less than $7\mu m$ could, according to these results, be suspended in the air indefinetly. For the $\overline{v^2}-f$ model the result was slightly different as particles up to $13\mu m$ could be suspended indefinetly. As the only significant difference between the SA and $\overline{v^2}-f$ models in this case is the the secondary flow (see Table 4.1) and figure 4.6, this clearly demonstrates the importance of secondary flow on the deposition rate.

That there exists a threshold value for each of the models is not surprising as the effect of gravity and turbulent fluctuations have been neglected, and so the inertia of the particles determine the deviation of the particle path from the streamlines of the flow field.

There does exist models in fluent that are designed to incorporate the effects of turbulent fluctuations in the calculations. These models are unforunately based on the turbulent time scale $\frac{k}{\varepsilon}$ which, we know from the previous section, becomes extremly large near the center of the chamber. This results in an extreme overprediction of the turbulent fluctuations. For this reason these models are not considered here.

Whilst simulations such as this do not yield a lot of information about the deposition rate of the particles smaller than the threshold value, it does tell us that that the particles with larger diameters will deposit rather quickly as the effect of gravitation and turbulent fluctuations are likely to increase the deposition rate rather than decrease it. The problem of determining the actual threshold value is however still unanswered. As the secondary flow field of the LES is even greater than that of the RSM and SA models, it is likely that the value is less

than $7\mu m$. Typical particle paths from these simulations are found in figure 4.9

The second part of the particle transport consisted of trying to model three dimensional case including gravity. The idea was to convert the 2d data for the flow field to 3d data by rotating it. Unfortunately no such proceedure existed in Fluent and so an algorithm that converts a 2d interpolation file to a 3d interpolation file had to be constructed. This algorithm is included in appendix A.

Unfortunately such an algorithm does not work close to the outer wall because of the finite prescision used to simulate the circular wall as well as because of the limited prescision of the 3-dimensional mesh. This means that the velocity data closest to the wall, where it is most crucial, is erroneous. The result of this was that all the simulations yielded that all particles would be deposited.

The approach was not entirely without merit however as it could be used to visualize the 3-dimensional mean particle paths in almost the entire domain. An example of such a path is displayed in Figure 4.10.

The LES flow field could also have been used to simulate the particle transport, but due to the time constraint this has not been attempted.

Even though the threshold values

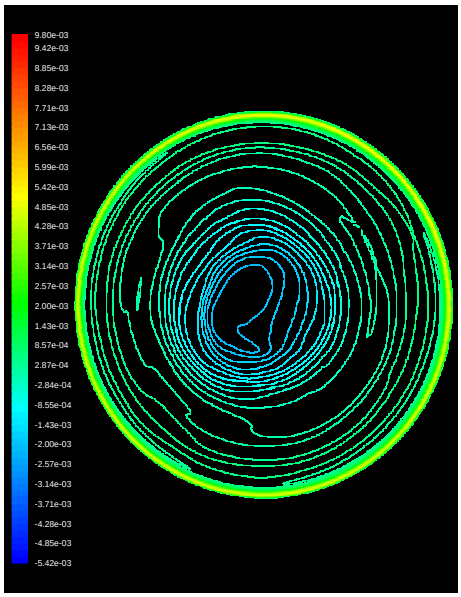

(a) Mean axial(x) velocity at x=0.05m

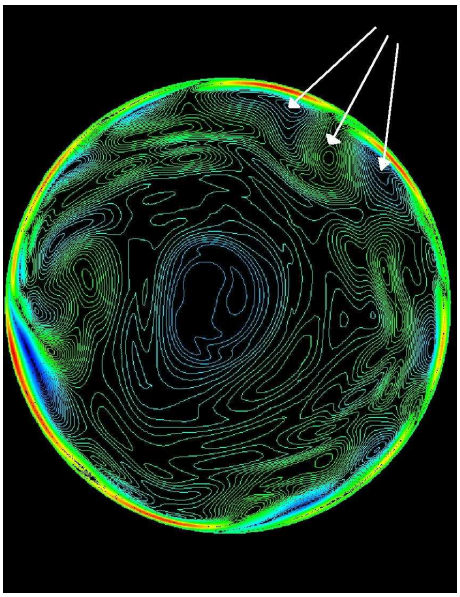

(b) Instantaneous axial(x) velocity at x=0.05m

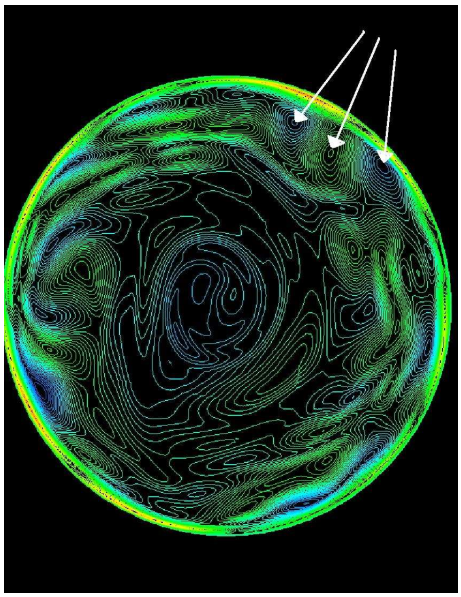

(c) Instantaneous axial(x) velocity at x=0.10m

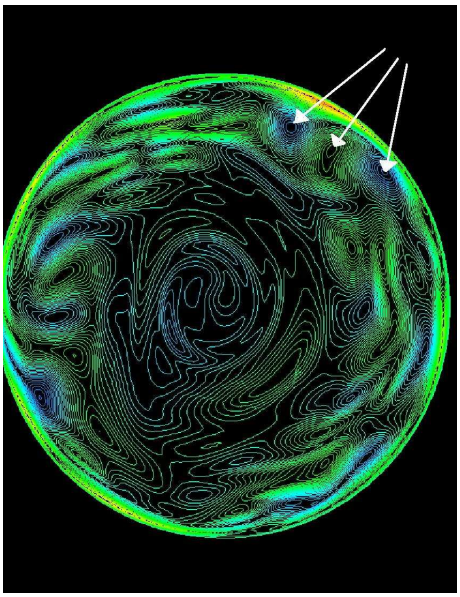

(d) Instantaneous axial(x) velocity x=0.15m

Figure 4.3: Contours of axial (x) velocity in the plane x=0.05

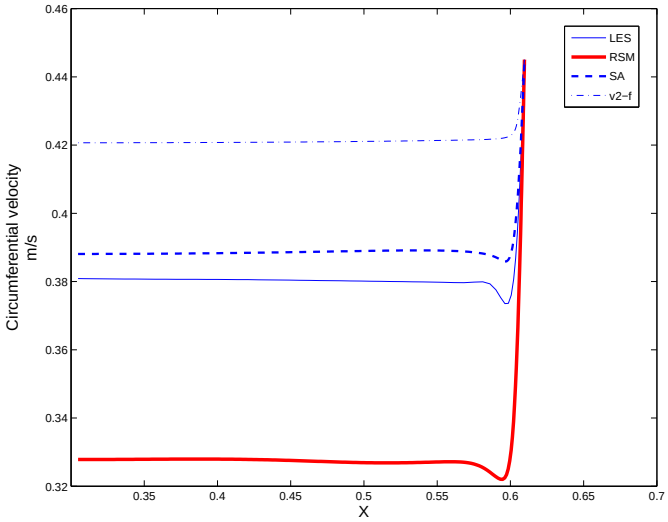

Figure 4.4: Circumferential velocity for RANS closures and mean Circumferential velocity for LES at the line $y = 0.85$

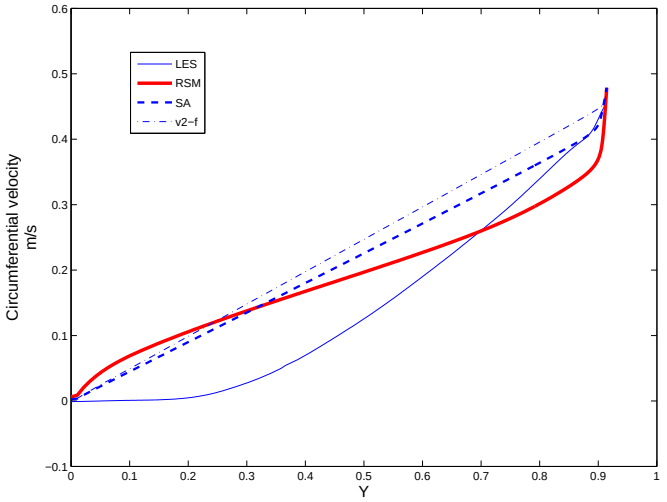

Figure 4.5: Circumferential velocity for RANS closures and mean Circumferential velocity for LES at the center of the chamber

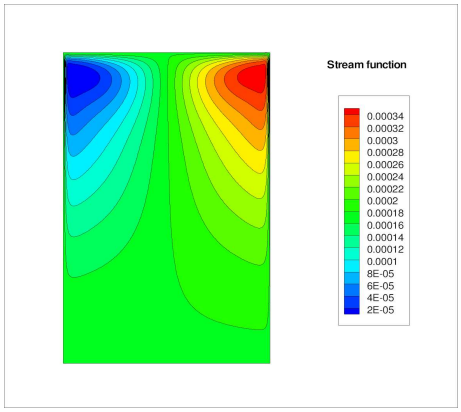

(a) Spalart-Allmaras

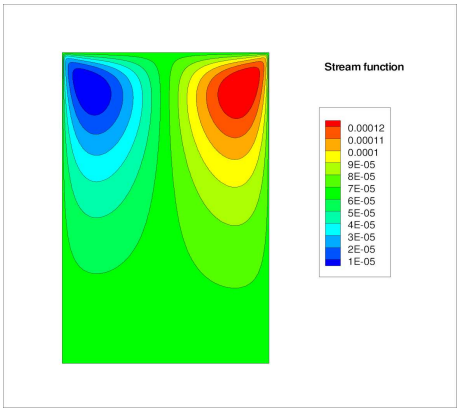

(b) $v^2 - f$

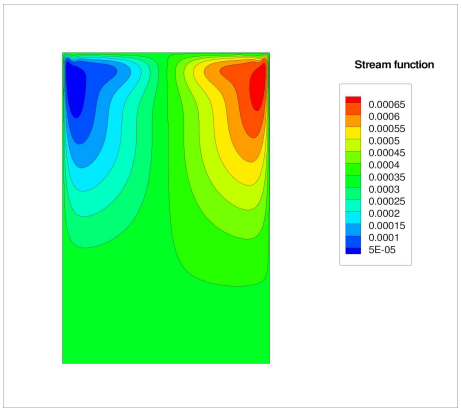

(c) RSM

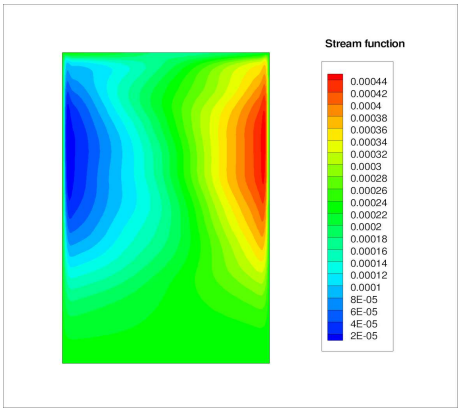

(d) LES

Figure 4.6: Contours of stream function in the plane z=0 $y \geq 0$

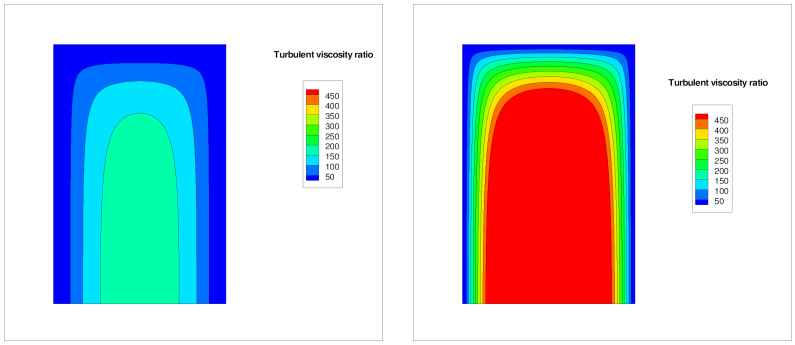

(a) Spalart-Allmaras (b) $\overline{v^2} - f$

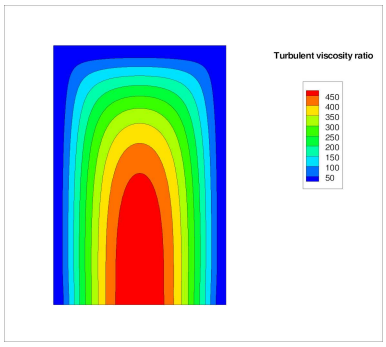

(c) RSM

Figure 4.7: Contours of Turbulent viscosity ratio in the computational domain

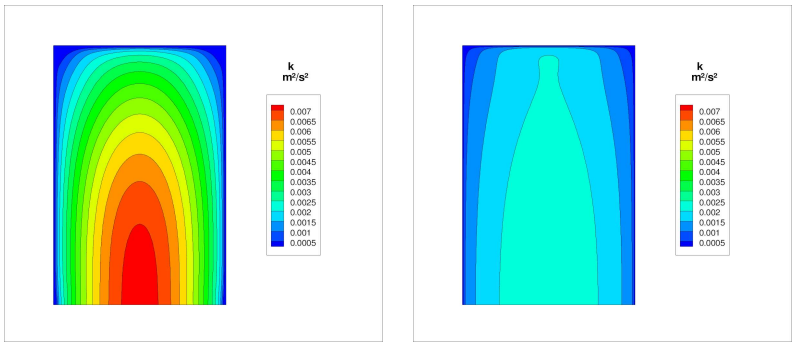

(a) RSM (b) $\overline{v^2} - f$

Figure 4.8: Contours of Turbulence kinetic energy in the computational domain

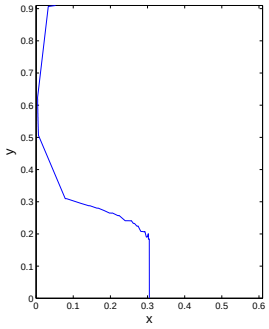

(a) Trajectory of a droplet of diameter greater than the threshold value released near the center of the chamber.

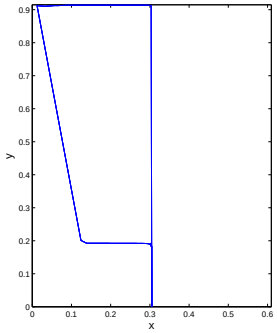

(b) Trajectory of a droplet of diameter less than threshold value released near the center of the chamber.

Figure 4.9: Particle paths for droplets in 2d simulations

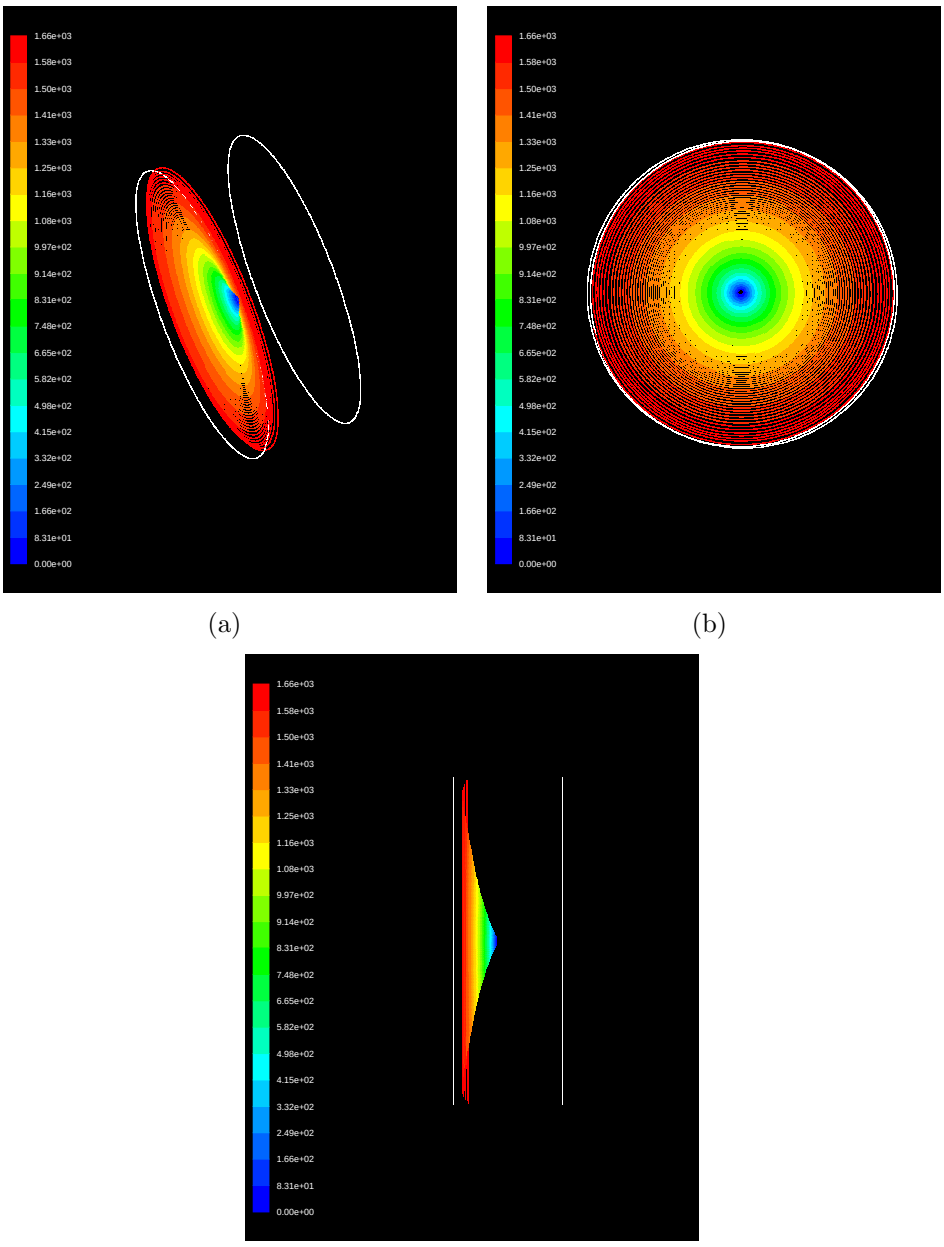

(a) (b)

(c)

Figure 4.10: Trajectory of particle in 3 dimensions viewed from different angels. The white circles are the disk shaped walls, and the legend indicates the residence time in seconds

Chapter 5

Concluding Remarks

In this project the complexity of the flow field inside the seemingly simple configuration of a steadily rotating aerosol chamber has been clearly demonstrated. Furthermore, we can conclude that none of the RANS models were able to reproduce the flow field predicted by the high resolution LES. The models did however produce holistically the same secondary flow fields which consisted of two counter rotating vortices. For all the models these predicted secondary velocities were smaller than the circumferential velocity by more than one order of magnitude. Moreover, all the models seem to predict Ekman boundary layers of the same thickness as the LES.

When it comes to particle transport, the predicted threshold size for what aerosols that could be suspended in the air for a significant amount of time was shown to be very dependent on the secondary flow. This means that the predictions of deposition made by the RANS models is highly uncertain. All of them do however let particles of considerable size be suspended, which is in accordance with observations. This might suggest that they can be used for such a purpose for some range of particle sizes.

For future study it would be interesting to see what the deposition rate would be for an instantaneous turbulent flow field. This could theoretically quite easily be conducted now that the LES velocity field has been obtained. If we are going to use the fluctuating field, however, the residence time of 10^3seconds approximated before makes this appraoch quite unfeasable from a computational demand point of view. Another interesting thing to consider would be the effect of changing the aspect ratio of the cylinder on the flow field, as this could have a dramatic effect on the secondary flow strength and thus significantly change the range of particles that could be suspended.

Bibliography

[1] Goldberg LJ. Naval Biomedical Research Laboratory, Programmed Enviroment, Aerosol Chamber. Applied Microbiology. 1971;21(2):244–252.

[2] Goldberg LJ, Watkins HMS, Boerke EE, Chatigny MA. The use of a rotating drum for the study of aerosols over extended periods of time. American Journal of Hygene. 1958;68(1):85–93.

[3] Frostling H. A rotating drum for the study of toxic substances in aerosol form. Journal of Aerosol Science. 1973;4(5):411–419.

[4] Asgharian B, Moss OR. Particle suspension in a Rotating Drum Chamber When the Influence of Gravity and Rotation are Both Significant. Aerosol Science and Technology. 1992;17(1):263–277.

[5] Gruel RL, Reid CR, Allemann RT. The optimum rate of drum rotation for aerosol aging. Journal of Aerosol Science. 1987;18(1):17–22.

[6] Durbin PA, Reif BAP. Statistical Theory and Modeling for Turbulent Flows. John Wiley and Sons; 2001.

[7] Kundu PK, Cohen IM. Fluid Mechanics. Academic Press; 2008.

[8] Spalart P, Allmaras S. A one equation turbulence model for aerodynamic flows. Technical Report AIAA-93-0439, American institute of Aeronautics and Astronautics. 1992;.

[9] Durbin P. Near-wall turbulence closure modeling without damping functions. Theoretical and Computational Fluid Dynamics. 1991;3:1–13.

[10] Kalitzin G. Application of the $v^2 - f$ model to aerospace configurations. Center for Turbulence Research Annual Research Briefs. 1991;.

[11] Heschl C, Sanz W, Klanatsky P. Implementation and comparison of different turbulence models for three dimensional wall jets with FLUENT. CFD Forum 2005. 2005;.

[12] Lilly Dk. A proposed modification to the Germano Subgrid-Scale Closure model. Physics of Fluids. 1992;4:633–635.

[13] Saffman PG, Turner JS. On the collision of drops in turbulent clouds. Journal of Fluid Mechanics. 1956;1(1):16–29.

[14] Inc F. Fluent 6.3 User's Guide. New Hampshire Press; 2006.

[15] Bradshaw P. 'Inactive motion' and pressure fluctuations in turbulent boundary layers. Journal of Fluid Mechanics. 1967;30(2):241–258.

Appendix A

Conversion code

This is the conversion code from a 2d interpolation file to a 3d interpolation file. It is written in java and the variable names are in Norwegian.

```
import easyIO.*;

class Konverterer{
 public static void main(String[] args) {
  int antallPunkter;
  int antallFelter;
  int Vinkel=1;
  String inntekst;
  In infil= new In("v2f");
     Out utfil= new Out("smc2");
     antallPunkter=finnAntall();
     System.out.println(antallPunkter);
     antallFelter=skrivOversikt(antallPunkter, Vinkel, infil, utfil);
     skrivXKoordinater(antallPunkter, Vinkel, infil, utfil);
     skrivYZKoordinater(antallPunkter, Vinkel, infil, utfil);
     skrivXKoordinater(antallPunkter, Vinkel, infil, utfil);
     skrivYZHastigheter(antallPunkter, Vinkel, infil, utfil);
     utfil.close();
 }
 static int finnAntall(){
  In innfil=new In("v2f");

  innfil.inLine();
  innfil.inLine();
  int antall=innfil.inInt();
  innfil.close();
  return antall;
 }
 static int skrivOversikt(int antall,
  int rotasjonsvinkel, In in ,Out ut){
  ut.outln(in.inLine());
  ut.outln("3");
  System.out.println("hei");
```

```
 rotasjonsvinkel=360/rotasjonsvinkel;
 antall=rotasjonsvinkel*antall;
 ut.outln(antall);
 in.inLine();
 in.inLine();
 antall=in.inInt();
 ut.outln(antall);
 for(int i=0; i<antall; i++){
  ut.outln(in.inLine());
 }
 return antall;

}

static void skrivXKoordinater(int antall, int rotasjonsVinkel,
In in, Out ut){
 rotasjonsVinkel=360/rotasjonsVinkel;
 String lest;
 for(int i=0; i<antall; i++){
  lest=in.inLine();
  for(int j=0;j<rotasjonsVinkel; j++){
   ut.outln(lest);
  }

 }

}
static void skrivYZKoordinater(int antall, int rotasjonsVinkel,
In in, Out ut){
     int n=360/rotasjonsVinkel;
      double[] Zkoordinater=new double[antall];
  double lest;
  int theta;
  int teller=-1;
  for(int i=0; i<antall; i++){
   lest=in.inDouble();
   theta=0;
   Zkoordinater[i]=lest;
   for(int j=0;j<n; j++){
    ut.outln(Math.cos(2*3.1415*theta/360)*lest);
    theta=theta+rotasjonsVinkel;
   }
  }
  for(int i=0;i<Zkoordinater.length;i++){
   theta=0;
   for(int j=0;j<n; j++){
   ut.outln(Zkoordinater[i]*Math.sin(3.1415*theta/180));
   theta=theta+rotasjonsVinkel;
   }
  }
}
```

```
 static void skrivYZHastigheter(int antall,
 int rotasjonsVinkel, In in, Out ut){
    double[] YHastigheter=new double[antall];
    double[] ZHastigheter=new double[antall];
    int n=360/rotasjonsVinkel;
    int theta=0;
    for(int i=0;i<antall;i++){
     YHastigheter[i]=in.inDouble();
    }
     for(int i=0;i<antall;i++){
     ZHastigheter[i]=in.inDouble();
    }
    for(int i=0;i<antall;i++){
      theta=0;
    for(int j=0;j<n; j++){
      ut.outln(YHastigheter[i]*Math.cos(2*3.1415*theta/360)
     -ZHastigheter[i]*Math.sin(2*3.1415*theta/360));
      theta=theta+rotasjonsVinkel;
    }
    }
    for(int i=0;i<antall;i++){
      theta=0;
    for(int j=0;j<n; j++){
     ut.outln(YHastigheter[i]*Math.sin(2*3.1415*theta/360)
     +ZHastigheter[i]*Math.cos(2*3.1415*theta/360));
     theta=theta+rotasjonsVinkel;
    }
         }
  }
}
```